NASA Contractor Report 187222

Engine Dynamic Analysis With General Nonlinear Finite Element Codes

M.L. Adams, J. Padovan and D.G. Fertis
University of Akron
Akron, Ohio

October 1991

Prepared for
Lewis Research Center
Under Grant NSG3-283

National Aeronautics and
Space Administration

TABLE OF CONTENTS

Section		Page
1.	INTRODUCTION AND BACKGROUND	1
2.	TIME-TRANSIENT NONLINEAR DYNAMIC ANALYSES	5
3.	OVERALL APPROACH USING INTERACTIVE ELEMENTS	7
4.	SQUEEZE-FILM DAMPER ELEMENT DEVELOPMENT	8
5.	METHOD OF DAMPER ELEMENT SOLUTION	11
6.	DEMONSTRATION OF DAMPER ELEMENT	15
7.	SQUEEZE-FILM DAMPER IMPLANT INTO ADINA - A DEMONSTRATION	18
8.	NUMERICAL CONSIDERATIONS AND EXAMPLES	20
	8.1 Benchmarking	20
	8.2 Explicit and Implicit Direct Integration Methods	21
	8.3 Demonstration Problems	22
9.	EXPERIMENTAL STUDIES	25
	9.1 Review of Some Recent SFD Studies	25
	9.2 Experimental Facility	28
	9.3 Experimental Method and Objectives	30
	9.4 Experimental Results	33
	9.5 Comparison with a Simplified Computer Model	34
10.	SUMMARY AND CONCLUSIONS	35
ACKNOWLEDGEMENTS		36
REFERENCES		37
NOMENCLATURE		40
ILLUSTRATIONS		41

FOREWORD

This report summarizes a three-year scope of work at the University of Akron within the field of transient/nonlinear dynamic analysis of gas turbine jet engine structures. Dr. C. C. Chamis was the NASA-Lewis Technical monitor of this grant. The focus of this work was on the development and implementation of rotor-stator interactive force elements for implant into general purpose nonlinear time-transient finite-element codes suitable for general engine dynamic simulation. The Principal Investigators on this grant were Drs. M. L. Adams*, J. Padovan and D. G. Fertis of the University of Akron. Graduate students involved with various portions of this work were I. Zeid, R. Quinn, E. Hirt, S. Payandeh and P. Lam.

* Now Professor of Mechanical Engineering at Case Western Reserve University, Cleveland, Ohio 44106.

1. INTRODUCTION AND BACKGROUND

There is currently a considerable interest and level of activity in developing computational schemes to predict general engine dynamic behavior. The general feeling among knowledgeable parctitioners working on engine vibration problems is that various modes of operation, such as blade-loss events, require a high level of analysis sophistication to realistically model the engine. Proper account of system nonlinearities (particularly at the bearings, dampers and rubs) appears to be necessary if analytical predictions are to be realistic. The approach used in this work makes use of already proven general finite-element nonlinear time-transient computer codes which are available on the open market. The work specifically described covers a three-phase NASA-Lewis sponsored research grant on engine dynamic simulation with available finite element codes. Phase -1 concentrated on the development of a bearing-damper element computer software package suitable for 'plug-in' to available finite element codes. Phase -2 focused on the implanting of this damper element into the ADINA code and extensive computational testing of the completed package. Phase -3 was related experimental work on a new test rig employing a flexible rotor mounted in two squeeze-film dampers.

Present-day jet engine configurations have evolved to a substantial degree through a trial-and-error process involving extensive testing. There are many fundamental dynamic phenomena which take place within these engines for which basic description and understanding have yet to be generated. Nonetheless, they work well. Modern aircraft engines are typical of current high-technology products in which the recently acquired computing capabilities of today are being used to better understand and improve what is

already designed, built and operating.

A better understanding of the basic dynamic characteristics of existing and new engine configurations is a prerequisite for producing acceptable engine efficiencies on advanced configurations (i.e., smaller rotor/stator running clearances). Also, a better definition of engine dynamic response would more than likely provide valuable information and insights leading to reduced maintenance and overhaul costs on existing configurations. Furthermore, application of advanced engine dynamic simulation methods could potentially provide a considerable cost reduction in the development of new engine configurations by eliminating some of the trial-and-error process done with engine hardware development.

The emergence of advanced finite element codes, such as NASTRAN, NONSAP, MARC, ADINA, ANSYS and ABAQUS and related algorithmic advances, has placed comprehensive engine system dynamic analyses within reasonable reach. What remains to be done is to develop new component element software to properly model engine rotor/stator interactive components, such as the squeeze-film damper, within the algorithmic logic of already proven finite element codes. This has been a major mission of this work.

For good reasons, aircraft gas turbine engines use rolling element bearings exclusively. This design philosophy had, in earlier times, deprived engines of the beneficial damping inherent in many other types of rotating machinery where fluid-film journal bearings are used. The implementation of squeeze-film dampers in later engine designs has now provided engine designers with an effective means of vibration energy dissipation. The net result is that engines with squeeze-film dampers are less sensitive to residual rotor imbalance and better able to control vibration

and transmitted force levels resulting from various excitation sources within the engine.

The field of rotor dynamics has evolved to its present state primarily through the solution to problems in classes of machinery older than aircraft engines. In most other types of rotating machinery (e.g., steam turbines, centrifugal pumps and compressors, fans, generators, motors, etc.) the rotor can be adequately modelled as an Euler or Timoshenko beam [1]. In addition, the support structure holding each bearing can often be adequately modelled as a separate mass-damping-stiffness path to ground (i.e., to the inertial frame). Also, for most purposes, bearing dynamic properties are characterized as stiffness and damping elements, linearized for small vibration amplitudes about some static equilibrium state. With few exceptions (e.g., Hibner [2]), it is this level of sophistication that has been utilized for the most part is rotor-dynamics analyses of aircraft engines.

Present day aircraft engines are structurally far more complex than most other types of rotating machinery. The multi-shaft configuration, plus the fact that the shafts are thin rotating shells, creates unique but significant complicating differences between aircraft engines and other turbomachinery. Also, the stator structural support at each rotor bearing represents anything but a separate mass-damper-stiffness path to an inertial frame. In fact, setting the inertial frame for the engine is not a simple matter when the full range of in-service maneuvers is realized. Dynamic paths between different bearings exist not only through the rotor but through several other paths within the nonrotating engine structure, i.e., a 'multi-level', 'multi-branch' system. As many as eight significant 'levels' have been identified.

The feasibility of nonlinear dynamic analyses of multi-bearing flexible rotors has been recently demonstrated on non-aircraft applications [3]. There are highly nonlinear dynamic effect in aircraft engines, particularly under large excitation forces, such as blade or disk failures, hard landings, and foreign matter ingestion events.

Clearly, the field of aircraft engine dynamics is presently in a position where there is both a need for substantial advances and feasible means available by which such advances can be accomplished.

2. TIME-TRANSIENT NONLINEAR DYNAMIC ANALYSES

In recent years it has become evident that an important class of engine dynamic phenomena can not be studied without accounting for the highly nonlinear forces produced at bearings/dampers, labyrinths and other close-running rotor/stator clearances under large amplitude vibrations. In such cases, linear theory typically predicts vibration amplitudes larger than the actual running clearances. Furthermore, important vibratory phenomena, such as subharmonic resonance and motion limit cycles, are 'filtered' out of the problem with a linear model, giving grossly erroneous predictions, qualitatively as well as quantitatively [3].

With few exceptions, nonlinear dynamics problems must be solved numerically as time-transient responses, whether the sought answer is a steady-state periodic motion or is strictly a transient phenomenon. The problem is mathematically categorized as an initial value problem in which the displacements and velocities of the complete system must all be specified at the beginning of the transient. From that point forward in time, the equations of motion are numerically integrated (known as 'marching') as far in time as one wishes to study the system motions and forces. If the system is dynamically stable, the transient motion dies out yielding the steady state response which in most real systems with a periodic force excitation will be a periodic motion. In a stable system with no time-varying force excitation, the transient will die out as the system comes to rest at one of its stable static equilibrium positions. If the system is unstable, the transient does not die out but continues to grow in time unless or until some nonlinear mechanism in the system limits the motion to what is frequently called a 'limit cycle' [3].

In order to study the general dynamical characteristics of aircraft engines, nonlinear dynamics computational schemes are required. The approach taken is to develop software packages to model engine components which are not typically found on dynamical structures and therefore are not already built into existing nonlinear finite element structural dynamics computer codes. The initial effort has concentrated on developing such a software package for squeeze-film bearing dampers.

3. OVERALL APPROACH USING INTERACTIVE ELEMENTS

Considering the typical engine structural complexities, an improved computational approach is necessary if a proper transient/steady-state model is to be developed for gas turbine engines. In this approach, it appears that the finite element method is one of the attractive modelling techniques for such problems. Its inherent capabilities include features essential to modern engines: 1) automatically handles multi-branch, multi-level structures in a more direct and efficient manner than flexibility approaches, 2) well-suited to handle nonlinearities associated with structural kinematic and kinetic effects [4], 3) easily accommodates various types of boundary and constraint conditions, and 4) easily accommodates material nonisotropy and nonlinearity [4,5]. A body of established and proven algorithms are available which can handle these various important effects [4,6] as well as geometric complexities, e.g., beam, plate, 2-D and 3-D elements [7].

The required features which were not previously available with general purpose finite-element codes are provisions to handle rotor/stator interactive forces originating from squeeze-film dampers, seals and rub/impact events. Presented in the next three Sections of this report are the results of an effort to develop a squeeze-film damper computer software package which can be 'plugged' into any existing finite element code.

4. SQUEEZE-FILM DAMPER ELEMENT DEVELOPMENT

The bearing damper element is essentially an interactive element to represent squeeze-film dampers. Its purpose is to bridge the 'gap' between structural elements which are separated in the actual engine by a squeeze-film damper. In its simplest version, it has an input/output setup as shown in Fig. 1. A source listing of this code is given in reference [8].

The rotor/stator interactive force generated in a bearing squeeze-film damper is modelled using an adaptation of the classical Reynolds lubrication equation for incompressible laminar isoviscous films.

$$\frac{\partial}{\partial x}\left(\frac{h^3}{\mu}\frac{\partial p}{\partial x}\right)+\frac{\partial}{\partial z}\left(\frac{h^3}{\mu}\frac{\partial p}{\partial z}\right)=6\frac{\partial}{\partial x}(hU)+12\frac{dh}{dt} \tag{1}$$

where,

z = axial coordinate

x = circumferential coordinate = rθ

h = local film thickness

dh/dt = instantaneous local rate of change in h

U = sliding velocity = Rω, typically zero in a damper

C = radial clearance of damper annulus.

The relationship between system inertial coordinates and damper parameters comes through the expressions for h, ∂h/∂x and dh/dt. Referring to Fig. 2, these relationships are summarized as follows:

$$\vec{e}=(X_R-X_S)\vec{i}+(Y_R-Y_S)\vec{j} \tag{2}$$

$$\dot{\vec{e}}=(\dot{X}_R-\dot{X}_S)\vec{i}+(\dot{Y}_R-\dot{Y}_S)\vec{j} \tag{3}$$

then

$$h=C-\dot{e}\cdot\hat{n}=C-(X_R-X_S)\cos\theta-(Y_R-Y_S)\sin\theta \tag{4}$$

$$\frac{\partial h}{\partial x} = \frac{1}{R}\frac{\partial h}{\partial \theta} = \frac{1}{R}\left[(X_R - X_S)\sin\theta - (Y_R - Y_S)\cos\theta\right] \tag{5}$$

and

$$\frac{dh}{dt} = -(\dot{X}_R - \dot{X}_S)\cos\theta - (\dot{Y}_R - \dot{Y}_S)\sin\theta \tag{6}$$

Many configurations of dampers which are currently being employed in engines have done away with centering springs common in older designs. Design simplicity as well as centering-spring fatigue life are apparently the major reasons. Also, in the majority of cases, damper end seals are used because this keeps damper throughflow sufficiently low to be compatible with the overall engine lub system of pre-damper configurations. However, the disadvantage of having end seals is that a 'large' damper clearance of typically 10 mils is required in order for the squeeze-film action to effectively dissipate vibration energy. From other considerations, a smaller damper clearance would be desirable (e.g., blade tip clearances). Without end seals, the optimum damper clearance is considerably smaller. Engines with higher oil flow capacity and no damper end seals are probably the trend on future designs.

Two typical configurations are shown in Figs. 3 and 4. The end seal configuration in Figs. 3 and 4(a) essentially divides the lubricant annulus into two pressure domains whereas that in Fig. 4(b) is a one-domain problem. In both cases, the 'long-bearing' solution is appropriate. Both solutions are options in the software package developed in this work.

For the 'long-bearing' solution $\partial p/\partial z \ll \partial p/\partial x$, and the following ordinary differential equation (two point boundary value problem) is obtained from equation (1), for U = 0.

$$\frac{d}{dx}\left(\frac{h^3}{\mu}\frac{dp}{dx}\right)=12\frac{dh}{dt} \tag{7}$$

For configurations with no end seals, an improved adaptation of the short-bearing approach is used by implementing the parabolic assumption of O'Donoghue [9]. The following approximation is made:

$$p(\theta,z)=p(\theta,0)\left(1-\frac{4z^2}{L^2}\right) \tag{8}$$

This assumes an axially symmetric axial pressure distribution at every circumferential location, and results in the following pressure field equation.

$$\frac{1}{\mu}\frac{\partial}{\partial x}\left(h^3\frac{\partial p}{\partial x}\right)=12\frac{dh}{dt}+8\frac{p(\theta,0)h^3}{L^2} \tag{9}$$

This is actually a first-order Fourier approximation using the parabola as the single approximative function.

A convergent approximation to the full two-dimensional Reynolds equation can be obtained, as an extension of the foregoing approach by O'Donoghue [9]. The number of Fourier terms is increased to N, resulting in N simultaneous ordinary differential equations.

$$p(\theta,z)=p_1(\theta,0)\cos\frac{\pi z}{L}+p_2(\theta,0)\cos\frac{3\pi z}{L}+\ldots+p_N(\theta,0)\cos\frac{(2N-1)\pi z}{L} \tag{10}$$

Substitution into the general 2-D Reynolds equation (1), followed by LHS:RHS segregation by arguments yields N ordinary differential equations, one for each $p_i(\theta,0)$, [9].

5. METHOD OF DAMPER ELEMENT SOLUTION

Although there are computationally fast closed-form solutions available such as given in [10,11], they do not retain sufficient generality to handle the specified pressure boundaries at supply and drain ports (Figs. 3,4,5) of typical configurations. Also, they are not amenable to structural deflections of the damper elements. For these reasons, the following approach has been used. Although somewhat computationally slower than closed-form solutions, it is nonetheless computationally quite efficient, and retains the generality deemed necessary. The solution method given below is used for all three formulations, i.e., equations (7) through (10). It is described below as implemented for the long-bearing formulation.

Based on a 3-point central difference, the following long-bearing equation yields equation (11).

$$h^3\frac{d^2p}{dx^2}+3h^2\frac{dh}{dx}\frac{dp}{dx}=12\mu\frac{dh}{dt}$$

$$\left(\frac{dp}{dx}\right)_i\cong\frac{P_{i+1}-P_{i-1}}{2\Delta x}$$

$$\left(\frac{d^2p}{dx^2}\right)_i\cong\frac{P_{i+1}-2P_i+P_{i-1}}{\Delta x^2}$$

$$h_i^3\left(\frac{P_{i+1}-2P_i+P_{i-1}}{\Delta x^2}\right)+3h_i^2\frac{dh_i}{dx}\left(\frac{P_{i+1}-P_{i-1}}{2\Delta x}\right)=12\mu\frac{dh_i}{dt} \qquad (11)$$

Rearranging (11) produces

$$\underbrace{P_{i-1}\left[\frac{h_i^3}{\Delta x^2}+\frac{3h_i^2}{2\Delta x}\frac{dh_i}{dx}\right]}_{D_i}+\underbrace{P_i\left[-\frac{2h_i^3}{\Delta x^2}\right]}_{C_i}+\underbrace{P_{i+1}\left[\frac{h_i^3}{\Delta x^2}-\frac{3h_i^2}{2\Delta x}\frac{dh_i}{dx}\right]}_{E_i}=\underbrace{12\mu\frac{dh_i}{dt}}_{R_i}$$

which is condensed to the following form:

$$C_iP_i+E_iP_{i+1}+D_iP_{i-1}=R_i \qquad (12)$$

Employing the recursion relationship,

$$P_{j-1} = A_j P_j + B_j \tag{13}$$

equation (12) can be expressed in terms of only two adjacent grid points as follows:

$$C_j P_j + E_j (A_j P_j + B_j) + D_j P_{j-1} = R_j \tag{14}$$

or

$$P_j (C_j + E_j A_j) + E_j B_j + D_j P_{j-1} = R_j \tag{15}$$

Therefore,

$$P_j = \left(\frac{-D_j}{C_j + E_j A_j} \right) P_{j-1} + \frac{R_j - E_j B_j}{C_j + E_j A_j} \tag{16}$$

which, when compared to equation (13), yields the following recursion relationships:

$$A_{j-1} = - \frac{D_j}{C_j + E_j A_j} \tag{17}$$

$$B_{j-1} = \frac{R_j - E_j B_j}{C_j + E_j A_j} \tag{18}$$

From the upstream boundary condition for each domain, the {A} and {B} vectors are determined by starting with $A_2 = 0$, $B_2 = P_1$ (called the forward sweep).

The downstream boundary condition is inserted at the beginning of the backward sweep as follows:

$$\begin{aligned} P_{M-1} &= A_M P_M + B_M \\ P_{M-2} &= A_{M-1} P_{M-1} + B_{M-1} \\ &\vdots \qquad\quad \vdots \\ P_2 &= A_3 P_3 + B_3 \end{aligned} \tag{19}$$

Film rupture is handled by the following substitution. If $P_j < P_{vapor}$, set

$P_j = P_{vapor}$ before computing P_{j-1}. This is equivalent to the condition $\partial p/\partial x = 0$ at the film-rupture full-film boundary. In the case of the 2-D convergent approach indicated by equation (10), this point-by-point test is made on the local summation.

$$P(\theta_i, z) = \sum_{k=1}^{i} P_k(\theta_j, z).$$

The method of solution, although not closed-form, is noniterative and is a 1-D adaptation of the 2-D finite difference method of Castelli and Shapiro [12]. While it does entail a one-dimensional, finite-difference scheme, it requires only a very small amount of CPU time and is therefore ideally suited to time transient rotor dynamics analyses. It has major advantages over the purely closed-form approximations, e.g., [10,11], as noted earlier. These major advantages are immediate account of specified-pressure boundary conditions at feed and drain holes of a damper. Also, the finite difference approach easily permits account of static as well as dynamic deflections which alter the oil film gap geometry from ideal rigid circular shapes.

Forces components on rotor are computed by numerical integration of the instantaneous film pressure distribution, as is standard.

$$\begin{aligned} F_i &= -\int_{A_i} \cos\theta dA = -LR\int_{\theta_1}^{\theta_2} p(\theta)\cos\theta d\theta \\ F_j &= -\int_{A_i} \sin\theta dA = -LR\int_{\theta_1}^{\theta_2} p(\theta)\sin\theta d\theta \end{aligned} \tag{20}$$

Stator force components are equal but opposite the rotor force components.

Force gradients (i.e., instantaneous tangent stiffness and damping) components are obtained by local 'small' perturbations, as is standard.

$$[C_{ij}]_{2\times 2} = \left[-\frac{\partial F_i}{\partial \dot{X}_j}\right]; [K_{ij}]_{2\times 2} = \left[-\frac{\partial F_i}{\partial x_j}\right] \tag{21}$$

where

$$\frac{\partial F_i}{\partial \dot{X}_j} \approx \frac{\Delta F_i}{\Delta \dot{X}_j}; \frac{\partial F_i}{\partial X_j} \approx \frac{\Delta F_i}{\Delta X_j} \tag{22}$$

Numerical differentiation is performed with small ΔX_j and $\Delta \dot{X}_j$ increments about instantaneous conditions. This provides continuous updating of $\{F_j\}$, $[C_{ij}]$ and $[K_{ij}]$.

6. DEMONSTRATION OF DAMPER ELEMENT

For purposes of checking out the damper element code (SQUEEZ) and to demonstrate its use, two types of computations were made. First, a parametric study of damper pressure distributions was made for a variety of specified circular orbits, for both long-bearing and short-bearing solutions. Second, a four-degree-of-freedom rotor-damper-stator model was investigated under conditions of small rotor unbalance through large rotor unbalance. These results are summarized.

For the parametric study on pressure distribution, the following damper annulus parameters were used:

Diameter, $D = 6$ in.

Length, $L = 1.25$ in.

Radial clearance, $C = 0.010$ in.

Lubricant viscosity, $\mu = 1 \times 10^{-6}$ reyns

Angle between inlet oil port and drain port, $(\theta_i - \theta_o) = 180$ deg

Inlet oil port pressure, $P_i = 55$ psia

Drain port pressure, $p_o = 15$ psia

Lubricant vapor pressure, $p_v = 1.5$ psia

Orbit angular velocity, $\Omega = 3600$ cpm (377.rad/sec)

The above damper parameters are typical for modern gas turbine aircraft engines. A parametric study was made postulating the outer ring of the damper fixed and the inner ring having a constant-radius constant-velocity concentric orbit. Eccentricity ratios (i.e., orbit radius/radial clearance) from 0.05 to 0.95 were computed, both for the long-bearing and short-bearing solutions.

Circumferential center-line pressures were plotted as a function of circumferential position and time, for one period of prescribed motion. The

results for the long-bearing solution are shown in Fig. 6, and for the short-bearing solution in Fig. 7. The difference between long-bearing and short-bearing solution is quite large when compared with the same radial clearance. One therefore sees why dampers with end seals require larger clearances to work properly than dampers without end seals.

A simple 'driver' code was written (see listing [8]) which uses the damper-element code in the same manner as a general implanted application with large finite element codes. The 'driver' code is based on a four-degree-of-freedom system, i.e., planar motion of the inner and outer damper elements. This then simulates a single-mass rotor connected to a single-mass stator through the damper element. The system analyzed is shown in Fig. 8. The model is coded to simulate arbitrary rotating and/or static radial loads. Aside from demonstration purposes, this four-degree-of-freedom model has been devised as a 'bench tester' of different damper models and configurations.

Note from Fig. 8 that the high-pressure port (i.e., feed port) is located on the bottom of the damper so as to assist 'lift-off'. Since centering springs are not typically used, they have been excluded in this example, being the most nonlinear type case and therefore computationally the most demanding of the algorithms employed. Lift-off therefore requires some amount of vibration to overcome the dead-weight load. Rotating unbalance loads of 100, 200, 300, 500, and 1000 lbs were run with Ω = 150 rad/s. Orbital plots were made showing rotor and stator total motion on one plot and rotor-relative-to-stator motion on a second plot. The plotted results are shown in Figs. 9 through 13.

For a 100 lb rotating load (Fig. 9) the motions shown are for a 20 load-cycle transient from time = 0. The rotor and stator each show close to

the same motion, and their relative motion is small, with the rotor barely 'lifting off'. The relative orbit is essentially oscillatory. However, when the rotating load is increased to 200 lbs, (Fig. 10), the relative orbital motion shows the beginnings of orbital motion, i.e., a 'crescent moon' shape as measured by numerous investigators. Further increase in magnitude of the rotating load to 300 lbs (Fig. 11) shows a well-defined steady-state total motion as well as relative motion. Note that with a 300 lbs rotating load, the relative (rotor-to-stator) orbit is still small in comparison to the radial damper clearance and confined to the region of the bottom of the damper. However, an increase of rotating load magnitude to 500 lbs causes a considerable change to the relative orbit (Fig. 12). Notice now that the relative motion of the rotor with respect to the stator fills a major portion of the clearance circle. Further increase of rotating load magnitude to 1000 lbs (Fig. 13) simply causes the steady-state relative orbit to expand and fill even more of the damper clearance circle.

7. SQUEEZE-FILM DAMPER IMPLANT INTO ADINA - A DEMONSTRATION

The squeeze-film damper element (SQUEEZ), described in previous Sections of this report, is also summarized in references [8] and [13]. Reference [8] also contains Fortran computer code listings for the damper element as well as for the four-degree-of-freedom driver code used in its development and demonstration.

To demonstrate the implementation of the SQUEEZ element into a general purpose transient nonlinear finite element (FE) code the ADINA code was purchased from MIT by the University of Akron as a cost-sharing expenditure. The next group of Sections in this report describe the implant of SQUEEZ into the ADINA code, a general purpose nonlinear FE code well known and used throughout the field of structural mechanics. This implant work is also summarized in references [14] and [15], with complete Fortran listings of all generated software and graphics packages given in reference [15].

To benchmark the approach described in references [14,15], the appropriate general purpose finite element code had to be selected. As noted in the first year report [13], the ADINA code was chosen for this purpose. This follows from the fact it has the requisite features required for rotor-bearing-stator simulations. These include: (i) Linear and nonlinear substructuring features, (ii) An extensive element library, (iii) Capability to handle kinetic, kinematic and material nonlinearity, (iv) Explicit and implicit integration loops, (v) Simplified I/O features, (vi) Accessible code architecture, (vii) Extensively benchmarked, and (viii) Requisite portability and general availability. In terms of the squeeze-film damper element noted in [8], extensive modifications were introduced into the ADINA code. These modifications were made general enough so as to handle rotor-bearing-stator simulations involving any number of rotors and associated

squeeze-film damper elements. The ADINA program has two available solution procedural loops, namely either explicit or implicit time-step integration of the equations of motion.

Since extensive amounts of data are generated during a typical run, graphics post processors have also been developed to simplify output evaluation. These include both 2-D as well as 3-D plotter schemes. The 2-D processor enables the plotting of: (i) Bearing/rotor trajectories at a given station, (ii) Stator trajectories, (iii) Clearance histories at given bearing stations, and (iv) Force, velocity and acceleration histories at given bearing stations. The 3-D processor enables the plotting of isometric views of the rotor trajectories. All these code listings are contained in reference [15].

8. NUMERICAL CONSIDERATIONS AND EXAMPLES

This Section describes the work pertaining to the computational characteristics of ADINA-with-SQUEEZ direct integration approach of FE generated rotor-bearing-housing motion simulations.

8.1 Benchmarking

To benchmark the overall procedure, a simple lumped parameter direct integration scheme was developed. This approach was used to check the accuracy of the FE generated scheme involving the ADINA-SQUEEZ 'implant'. As the first example of such benchmarking, consider the system defined in Figure (14). The material and geometric properties associated with the dual ported squeeze-film damper bearing employed in this and the following sample problems are defined by

Nominal diameter = 6 inches,

nominal length = 1.2 inches,

Clearance = 1. inch, viscosity = $.1*10^{-5}$,

film rupture pressure = 15 psia,

$\theta_1 = 90$, $\theta_2 = 270$, $P_1 = 15$ psi, $P_2 = 55$ psi. Note as with current practice, the bearing used in the simulation has no centering spring. In terms of this system, Figs. (15-17) illustrate various aspects of the validation of the Newark [16], Wilson [17] and central difference generated results with those of the benchmark. In this way, both the implicit and explicit schemes are treated. In each of the comparisons, three different aspects of rotor bearing stator behavior are depicted specifically.

a) Rotor displacement trajectories,

b) Stator displacement trajectories, and

c) Relative rotor orbit.

For the present purposes, while extensive benchmarking was undertaken, for convenience, only the case of mild rotor unbalance is depicted. As can be seen, for the given Δt steps chosen, good comparisons were obtained by both the implicit and explicit schemes. Such benchmarking was obtained over a wide range of rotor speeds and rotor unbalance levels. In all cases, good accuracy was yielded. Similar benchmarking was also performed for multi-bearing-rotor-stator simulations. Note, so long as Δt was kept small, good accuracy was obtained over a wide range of system variables.

8.2 Explicit and Implicit Direct Integration Methods

For problems involving few degrees of freedom, it was found that for a given accuracy, both the implicit and explicit schemes required about the same overall computational times. This follows from the fact that for 'small problems', the architectural overhead associated with the implant strategy programming dominates over the relative algorithmic efficiency. Note for transients initiated by rather severe unbalance loads, it was found that the implicit scheme proved to be more sensitive to the choice of time step size. Interestingly, such sensitivities were found to occur for problems with small as well as large numbers of degrees-of-freedom. After performing several parametric studies, it was found that during the course of a typical transient, particularly involving a severe loading, the tangent properties of the fluid film undergo major changes. Because of this, a perfusion of system harmonics are introduced into the transient response as the tangent fluid film properties vary. Note, this behavior is intrinsic to the fluid film and hence, is independent of the number of degrees-of-freedom of the rotor-stator model. Such properties tend to reduce the stability threshold of the implicit scheme which is best employed when only a few harmonics

are excited. For problems involving large numbers of degrees-of-freedom, the sensitivity of the implicit scheme coupled with the required continuous updating and inversions of the dynamic stiffness tends to reduce the running efficiency of the procedure. In contrast, the central difference approach tends to be less sensitive to such tangent property fluctuations. This is true so long as the resulting family of harmonics is bound by the spectral characteristics of the rotor-stator system. Because of this, similar Δt can be employed by the implicit and explicit scheme. In this context, the explicit scheme has a somewhat better computational efficiency than the implicit approach. This follows from the fact that no continuous inversion is required by the explicit scheme.

8.3 Demonstration Problems

To demonstrate the various capacities of the ADINA implant strategy, the results of several example problems will be considered. This will involve single and multiple bearing problems with various types of rotor unbalance histories, impact events and rotor speeds. For example, in terms of the single bearing system given in Fig. (14), Figs. (18 and 19) illustrate various aspects of the response histories to an imbalance load which is applied as a ramp function in time. As this loading is more severe than that applied in Figs. (15-17), the rotor tends to fill its clearance circle as seen in Fig. (19). If the same system is subject to a unidirectional impulse, as might be expected from a rough landing, Figs. (18) and (20) illustrate the associated response history. By comparing Figs. (18) and (20), the effects of the impulse can be clearly seen from the ovalizing of the rotor trajectories. This is directly due to the directional characteristics of the impulse load. Note, comparing the results in Fig. (19), we

see that the rotor orbits are essentially unchanged by the presence of the shock load. Hence, it follows that the squeeze-film damper has essentially no effect on mitigating the worst aspects of unidirectional shocks when large unbalances are simultaneously present.

The next series of examples pertains to the rotor-bearing-stator system defined in Fig. (21). To simulate the shafting, the beam elements available in the ADINA system are utilized. Note, the mass effects are handled via the lumped parameter approach. Figs. (22) and (23) illustrate the effects of increasing the severity of loading on the dynamic response of multi-bearing problems. As can be seen, increasingly stiffer squeeze-film damper responses are excited. Note, as the load is further increased, the rotor stator tranjectories become 'locked in'. The next series of Figures, namely (24-25), illustrate the effects of suddenly applied rotor unbalances. Since the rotor speed considered is high, only a small portion of the clearance circle is filled. This follows from the fact that due to the rather rapid changes in orientation of the exciting load, inertia filtering occurs. Because of this, the rotor is supported by severe velocity gradients which are only in a close neighborhood. Hence, the pressure gradient generated by the inlet and outlet ports of the squeeze-film device causes the rotor to settle in the direction of the low pressure port. Note, as the rotor speed is decreased, increasingly larger rotor orbits occur. Similar trends occur as the level of unbalance is increased.

Based on numerous parametric studies involving systems similar to the foregoing, it was found that all the time integration schemes considered were stable for situations wherein the fluid underwent only moderate changes in stiffness during the overall cycle. Eventhough a perfusion of harmonics is introduced by even moderate changes in stiffness (so long as the result-

ing spectra are strongly bound by the frequency envelope of the dominate system frequencies), spurious energy flow to higher order modes is insignificant. Specifically, for the implicit scheme, if the choice of time step size is gauged to the dominate higher order system frequencies, then the introduction of lower order spectra by the squeeze-film has little effect on numerical stability. In contrast, if strong stiffness modulations occur, the significant amounts of energy flow are introduced in the ever shifting higher order modes. This leads to solution instabilities unless smaller Δt are introduced. In this context, the use of the explicit scheme is advocated over the implicit for problems involving strong-to-weak unbalance loads.

9. EXPERIMENTAL STUDIES

This Section of the report summarizes the third (final) year work on this grant. This effort was focused primarily on basic experimental studies on the orbital vibration characteristics of uncentralized (i.e., no centering spring) squeeze-film dampers supporting a flexible rotor. The objectives of this work were (i) to conceive, design and build a new test apparatus involving two squeeze-film dampers supporting a significantly flexible rotor, (ii) to perform a wide variety of experimental parametric studies with the apparatus, and (iii) make fundamental comparison with computational results based on mathematical models and computer algorithms developed in the previous two phases of this grant. These objectives are summarized as follows:

- Conceive, design and construct test rig
- Experimental parametric study
- Comparisons with computational results

The squeeze-film damper (SFD) work summarized in this Section is presented with considerably more detail in reference [31], the MSME thesis of R.D. Quinn.

9.1 Review of Some Recent SFD Studies

In 1970, Gunter published an investigation concerning the determination of the desirable values of rolling element bearing support stiffness and damping for rigid rotors [18]. The mathematical model simulated a general four degree-of-freedom unbalanced rotor mounted on two damped, linearly flexible supports. The stiffness and damping coefficients could be constant or speed dependent.

In 1973, Giberson [19], of Turbo Research Inc., published a paper acclaiming the ability of SFD to stabilize otherwise unstable rotors supported with journal bearings. When rotor speed surpasses the threshold of instability for the journal bearings, 'whirl' amplitude theoretically grows without bound, possibly destroying the machine. Pivoted pad journal bearings can stabilize a system by themselves, but 'pivoted pad bearings supported by SFD is the arrangement with the greatest ability to stabilize a rotor bearing system that uses hydrodynamic bearings'.

In 1974, Mohan and Hahn [20] published a paper on the 'Design of SFD Supports for Rigid Rotors'. The publication includes a general design guide for centrally preloaded SFD, supporting a rigid rotor, mounted on rolling contact bearings. The authors also investigated the transient solutions of the fully non-linear equations of motion to discover the effect of central preloading.

In 1975, Cunningham, Fleming, and Gunter [21] published an analytical investigation on the design of a centrally preloaded SFD for a multimass flexible rotor mounted on rolling contact bearings. The paper demonstrates a technique for the use of single mass, symmetric, flexible rotor analysis to optimize the stiffness and damping for a symmetric five mass rotor. The single mass analysis was taken from a 1972 NASA Report by Kirk and Gunter.

In 1979, Tonneson [22], of the Technical University of Denmark, published a study on experimental squeeze-film bearing orbits. The purpose of the investigation was to compare experimentally measured damping coefficients with those obtained from simple linearized theory. Comparisons were made to both eccentric (offset) and concentric (centralized) damper journal orbits.

In 1977, Bansal and Hibner [23], of Pratt and Whitney, published an 'Experimental and Analytical investigation of (dynamic) SFD Forces Induced by Offset Circular Whirl Orbits'. In agreement with Tonneson, the authors suggest that offset orbits are more realistic for flexible damped supports.

In 1977, Hibner, Bansal and Buono [24], of Pratt and Whitney, published a paper on the control of instability for the intershaft SFD. An earlier analytical and experimental investigation had shown the existence of an intershaft viscous damper instability.

In 1979, Hahn [25] published an analytical investigation on the 'Unbalance Behaviour of Squeeze Film Supported Rigid Rotors'. Equilibrium load capacity and transmissibility data for a wide range of operating conditions are presented for centrally preloaded and unloaded vertical rigid rotors mounted on rolling element bearings.

In 1979, Vance [26], of Gas Turbine Laboratories, published a review of rotor dynamics which included the current role of SFD as a solution to dynamical problems.

In 1979, Hibner and Bansal [27] published an experimental and theoretical investigation into 'The Effects of Fluid Compressibility on Viscous Dampers'. The investigation was begun because of the questionable validity of the Reynolds equation when cavitation exists in the squeeze film. The effects of cavitation could explain why correlations between theory and experiment for SFD have been excellent in some cases and poor in others.

In 1979, Holmes [28], of the University of Sussex, U.K., published a study on the control of rotor vibration using SFD with and without a parallel flexible element. The experimental and analytical investiga-

tion includes a general design philosophy.

In 1980 and 1981, Cookson and Kossa [29,30] published the results of their experimental and analytical investigations into the effectiveness of SFD, without parallel flexible supports, used for supporting flexible rotors.

9.2 Experimental Facility

The rotor system was designed for use on a Bently-Nevada rotor dynamics test rig. The rotor was powered by a 1/10 horsepower infinitely controllable drive motor capable of driving the test rotor at speeds in excess of 10,000 RPM. The system included a shaft supported by two sets of preloaded duplex ball bearings, with each duplex set mounted in an uncentralized SFD. A quill shaft was used to couple the motor and rotor. Rotor discs of various weights could be located at any position between the bearing stations (see Figs. 26 and 27).

The preloaded duplex ball bearings provided for stiff bearing-rotor coupling, so that the bearings could be assumed to be rigid in comparison with the rotor and damper film. The preload on the bearings also increased the rolling friction which decreased the maximum attainable rotor speed and increased heat generation.

The ball bearing housings which preloaded the duplex bearings acted as the damper journals. The damper journal diameters were 3.3125 inches, the journal land lengths were .475 inches. So, the length to diameter ratio was .143, suitably short for a short bearing approximation of the Reynolds equation to apply.

The damper housings had interchangeable inserts allowing the radial clearance for the fluid annulus between the damper bearings and journal to

be varied from .004 to 0.20 inches. Sealing between the journal and damper bearing was accomplished with O-rings in shear. The lateral clearance between the damper journal and housing was dimensioned to yield .007 inches of 'squeeze' on each O-ring. This amount of O-ring squeeze was determined with a trial and error approach to be near the optimum, sealing adequately under the required oil pressure yet contributing minimal impedance to journal motion. Circumferential grooves with outlet ports were located in the sides of the damper housings at the edges of the fluid film annulus. Ports were also provided to check the static oil pressure in the grooves at the end of the annulus with a pressure gauge. Also, inlet and outlet ports were located centrally in the damper inserts and housings at the top and bottom of the dampers. Flow metering valves at the outlet ports allowed for the end seal or no end seal conditions (or any amount of end leakage or end pressure desired). On/off valves at the inlet ports allowed for circumferential groove or port oil feed into the damper annulus. With the appropriate ports closed or open, the damper configuraiton could be modelled validly by either the short or long bearing approximation of the Reynolds equation. An antirotation pin was threaded through the outside of the damper housing, through the inserts and into an oversized hole in the journal, allowing journal translation but not rotation (see Fig. 28). Also, see Figs. 28 through 32 for more details on the various specially designed damper and other parts.

The steel rotor shaft was 13/16 inches in diameter and 12 inches long between bearings. The quill shaft used as the flexible coupling between the motor and the rotor was 6 inches long and an 1/8 inch in diameter. See reference [16] for the rotor and quill sizing calculations. The flexible

coupling eliminated the need for exact alignment of the motor and the two rotor bearings. Two rotor discs could be located at any position between the bearings with set screws. Each rotor disc had threaded holes through its thickness located symmetrically about its outside circumference for the positioning of balancing weights. The discs were modelled after those that were furnished with the Bently-Nevada test rig. With both discs axially centered on the shaft, the first flexible mode could be excited.

A gear pump was used to pump the oil from a heated bath through the SFD. A metered bypass line provided a wide range of damper inlet pressure and flow rate. Heating the SAE 10W oil provided a wide range of damper fluid viscosity. Copper-Constantan thermocouples were used to monitor the oil inlet and outlet temperatures from the dampers. A thermal well was used for monitoring the pressurized inlet temperature.

Vibration detection was accomplished with Bently-Nevada non-contacting proximity displacement transducers. The output of the proximitors was wired into a digital vector filter (DVF2) also manufactured by Bently-Nevada. The DVF2 provided a digital readout of peak to peak displacement, RPM, and phase angle for location of the rotor's 'high spot' for balancing. Two Tektronix oscilloscopes, an X-Y-Y plotter, and an HP spectrum analyzer were also useful aids in studying and recording vibraitonal response. The spectrum analyzer was expecially useful for investigating nonsynchronous responses. A five thermocouple input, digital readout potentiometer was used to monitor oil temperature into and out of the SFD. The schematic diagram for this assembly is shown in Fig. 33.

9.3 Experimental Method and Objectives

The initial purpose of the experimentation was to verify that the test

apparatus could work properly as designed and that operational data could be taken as desired. Once the system was debugged, the next step was to conduct a brief parametric study.

The parameters that could be contolled for both the 'short' and 'long' bearing configurations of the damper were as follows:

1) rotor speed

2) unbalance

3) clearance

4) oil temperature

5) oil inlet pressure

The second purpose was then to discover the effect on the rotor system's performance of varying each parameter while holding the others constant. Comparisons could then be made with other authors' results and with a simplified analysis and conclusions made.

The third and final purpose was to recommend possible improvements to the test equipment and to suggest further work.

Bode plots of peak-to-peak amplitude and phase vs. rotor speed could be made at both damper locations and at any point along the shaft for both x and y positions. Also, damper and shaft orbits could be obtained and photographed for a particular rotor speed. The orbits (oscilloscope tracings) have a gap in them made by a reference mark useful for phase studies. The phase mentioned here is the angle between the high spot of the rotor and a reference mark on the shaft. The meaningful information is the change in this angle with speed (denoting changes of angles between the high spot and the unbalance position).

The first task was to balance the rotor after the system was assembled

with the null-clearance inserts in the dampers providing 'rigid' bearing supports. The DVF2 aided in this endeavor. Fig. 34 shows the midspan vibrational response for the balanced rotor. Note that all Bode plots were made from a location two inches from the midspan location. Comparing with the other plot on the same Figure for a small unbalance, it can be seen that the residual unbalance is small. The sharp critical speed response on Fig. 34 and the abrupt phase change shown on Fig. 35 for a small unbalance demonstrates the high stiffness and lack of damping of the ball bearings. The first critical speed of the rotor can be seen to be about 9200 RPM.

In practice, the four damper mounting screws on each SFD were used to adjust the O-ring squeeze to seal adequately, yet contribute minimal impedance to journal motion. Shims were then required to restrain the damper bearings from vibrating relative to their respective housings.

When damper orbit studies were made, the GAP button on the DVF2 was used to obtain the approximate orbit center coordinates within the clearance circle. The GAP button provides a measure of the distance between the proximeter probes and the rotor. This method was also used to measure the radius of each clearance circle.

Fig. 36a and b are examples of typical photographs of the damper and shaft orbits respectively, taken from oscilloscope tracings. The rotation of the shaft is clockwise with respect to all orbits presented in this paper. Copies of each orbit photograph of interest were reduced to their proper scale, and placed in the correct position and orientation on drawings of their particular clearance circle. This was done because knowledge of the location (offset from center) of the orbit within the clearance circle was found to be useful.

9.4 Experimental Results

The complete set of experimental results are presented in reference [16] for the rotor system supported by SFD without end seals (annular oil inlet/outlet) and with end seals (port inlet/outlet). A summary of these follows.

Fig. 37, a superpositioning of four separate damper orbits, shows the effects of changing the unbalance while holding the other parameters constant. Increasing the unbalance increased the vibration of the rotor which resulted in a further 'lifting off' of the dampers from the bottom of the clearance circle as well as larger elliptical orbits.

Figs. 38 through 42 show amplitude plots of the rotor's x-axis for different values of unbalance. Note that the trends are consistent despite the clearance size. All cases show that at least as a small amount of effective damping was present, yielding a response superior to the 'rigid' response of Fig. 34. This is apparent from the lower amplitudes and the less abrupt phase shifting with additional dissipation. As more unbalance was applied, larger orbits were observed and the effective damping increased, displaying the amplitude dependent damping characteristics of the SFD. As noted by Cookson and Kossa for this type of dampers, the critical speed did not change appreciably. This shows that SFD act only as energy dissipators not as springs in series with the rotor. Note that the resonance peaks are not well defined, appearing as eroded versions of what they might have been with 'rigid' supports. The onset of a noise which was taken to be that of cavitation was noted at the peaks where the 'erosion' begins. Comparing the plots for the various clearances, it can be seen that larger clearances yielded freer motion of the damper journals and thus

'softer' dampers. Larger clearances yielded more favorable rotor responses (for this system).

9.5 Comparison with a Simplified Computer Model

The rotor was modelled using an available code, assuming the rotor to be rigid [8]. Of course, the rotor was not rigid at the speeds which the experimental results were obtained. Thus, the damper excitation was not necessarily the same and direct comparisons could not be made. However, qualitative comparisons concerning the general character of the orbits were found to be useful. All computed cases presented were run at 10,000 RPM, with 3 gm unbalance and low inlet pressure using a short bearing approximation of the Reynolds equation.

Considering Figs. 43, 44, and 45, with increasing viscosity, the orbit's amplitudes and offsets decreased, showing the damper to be growing stiffer. This agrees with the experimental results. Also, as the offset decreased, the orbits became more circular, which also agrees with experimental evidence. All of the computer produced orbits (clockwise rotations) are left of center (e.g., see Fig. 44) and approach the center line (y-axis) with decreasing offset. This is also the general rule for the experimentally obtained orbits. From this last comparison it can be seen that increasing the clearance in both cases produced larger orbits and offsets and thus a softer damper.

10. SUMMARY AND CONCLUSIONS

Phase -1 of this work provided the following:

- Overall solution strategy for the general engine dynamics problem
- Clear definition of where current efforts should be concentrated
- A SFD software package ready for FE implant

Phase -2 of this work provided the following:

- Methodology for implanting SFD element into a general FE code
- Benchmarking the SFD/ADINA combination
- Numerous relevant example-problem solutions

Phase -3 of this work provided the following:

- Conception, design and construction of a SFD/flexible rotor test rig
- The results of basic experimental parametric studies
- Comparisons with computed results and results of previous investigators

It is concluded that general engine dynamic analyses as a standard design-study computational tool is readily available, practical and highly desirable for the prediction and understanding of complex engine dynamic behavior. Improved definition of engine dynamic response will likely provide valuable information and insights leading to reduced maintenance and overhaul costs on existing engine configurations. Furthermore, application of advanced engine dynamic simulation methods will provide a considerable cost reduction in the development of new engine designs by eliminating some of the trial-and-error process done with engine hardware development.

Clearly, the field of aircraft engine dynamics is presently in a position where there is both a need for substantial advances and feasible means by which such advances can be accomplished. The necessary approach and methods have been developed, proven and demonstrated by this work.

ACKNOWLEDGEMENTS

The original idea for this work came from Dr. C.C. Chamis, the NASA Technical Officer and monitor of this grant. The authors greatly appreciate not only his inspired exposure of this general problem area but also his helpful suggestions and continued encouragement for all the investigators working on the grant.

We also appreciate the opportunity provided by NASA in its sponsorship of this grant. Not only have important methods and results been generated by this work, but also the professional learning experience for the principal investigators and involved graduate students has been quite significant. All of these individuals have gained much toward their continued professional growth and increased knowledge about an important aerospace field.

REFERENCES

1. D.G. Fertis, Dynamics and Vibrations of Structures, Wiley, New York, 1973.

2. D.H. Hibner, 'Dynamic Response of Viscous-Damped Multi-Shaft Jet Engines', AIAA Journ. of Aircraft, Vol. 12, 1975, pp. 305-312.

3. M.L. Adams, 'Nonlinear Dynamics of Flexible Multi-Bearing Rotors', Journ. of Sound and Vibr., Vol. 71, No. 1, 1980, pp. 129-144.

4. T. Belytschko, 'Nonlinear Analyses-Descriptions and Numerical Stability', Computer Programs in Shock and Vibration, ed. W. Pilkey and B. Pilkey, Shock and Vibration Information Center, Washington, D.C., 1975, p. 537.

5. O.D. Zienkiewicz, The Finite Element Method, McGraw Hill, London, 1977.

6. C.A. Felippa, and K.C. Park, 'Direct Time Integration Methods in Nonlinear Structural Dynamics', presented at FENOMECH, University of Stuttgart, 1978.

7. Structural Mechanics Computer Programs, ed. by W. Pilkey, K. Saczalski, and H. Schaeffer, University Press of Virginia, Charlottesville, 1975.

8. M.L. Adams, J. Padovan, and D.G. Fertis, 'Finite Elements for Rotor/Stator Interactive Forces in General Engine Dynamic Simulation, Part 1: Development of Bearing Damper Element', NASA Report on Grant NSG-3283, October 1980.

9. J.P. O'Donoghue, P.R, Koch, and C.J. Hooke, 'Approximate Short Bearing Analysis and Experimental Results Obtained Using Plastic Bearing Liners', Proc. Institute of Mech. Engineers, Vol. 194, 1969, pp. 190-196.

10. S.M. Rhode, and D.F. Li, 'A Generalized Short Bearing Theory', ASME Journ. of Lubrication Techn., Vol. 102, No. 3, 1980, pp. 278-282.

11. L.E. Barrett, P.E. Allaire, and E.J. Gunter, 'A Finite Length Bearing Correction Factor for Short Bearing Theory', ASME Journ. of Lubrication Techn., Vol. 102. No. 3, 1980, pp. 283-290.

12. V. Castelli, and W. Shapiro, 'Improved Method for Numerical Solutions of the General Incompressible Fluid Film Lubrication Problem', ASME Journ. of Lubrication Techn., Vol. 89, No. 2, 1967, pp. 211-218.

13. M.L. Adams, J. Padovan, and D.G. Fertis, 'Engine Dynamic Analysis with General Nonlinear Finite-Element Codes, Part 1: Overall Approach and Development of Bearing Damper Element', Trans. ASME Journ. of Engineering for Power, Vol. 104, July 1982, pp. 586-593.

14. J. Padovan, M.L. Adams, D.G. Fertis, I. Zeid, and P. Lam, 'Engine Dynamic Analysis with General Nonlinear Finite Element Codes, Part 2: Bearing Element Implementation, Overall Numerical Characteristics and Benchmarking', ASME Paper No. 82-GT-292, Presented at 1982 Gas Turbine Conference.

15. J. Padovan, M. Adams, J. Fertis, I. Zeid, and P. Lam, 'Engine Dynamic Analysis with General Nonlinear Finite Element Codes, Part II - Bearing Element Implementaiton, Overall Numerical Characteristics and Benchmarking', NASA Report on Grant NSG-3283, October 1981.

16. N.M. Newmark, 'A Method of Computation for Structural Dynamics', J. Eng. Mech. Div., ASCE, 85, EM3, 67-94 (1959).

17. E.L. Wilson, 'A Computer Program for the Dynamic Stress Analysis of Underground Structures', Report No. SESM68-1, Dept. of Civil Engineering, University of California, Berkeley (1968).

18. E.J. Gunter, 'Influences of Flexibly Mounted Rolling Element Bearings on Rotor Response, Part I - Linear Analysis', Journ. of Lubrication Techn., Vol. 92, Series E, No. 1, January 1970, pp. 59-69.

19. M. F. Giberson, 'Taming Rotor Whirl with Film-Damper Bearings', Machine Design, Vol. 45, No. 7, March 22, 1973, pp. 176-181.

20. S. Mohan and E.J. Hahn, 'Design of Squeeze Film Damper Supports for Rigid Rotors', J. Engr. for Ind., Trans. ASME, Series B, Vol. 96, 1974, pp. 976-982.

21. R.E. Cunningham, D.P. Fleming, and E.J. Gunter, 'Design of a Squeeze film Damper for a Multimass Flexible Rotor', J. Engr. for Ind., Trans. ASME, B97 (4), pp. 1383-1389 (1975).

22. J. Tonnesen, 'Experimental Squeeze Bearing Orbit Studies', J. Engr. for Ind., Trans. ASME, B97 (4), pp. 83-95.

23. P.N. Bansal and D.H. Hibner, 'Experimental and Analytical Investigation of Squeeze Film Bearing Damper Forces Induced by Offset Circular Whirl Orbits', Journ. of Mech. Design, Vol. 100, No. 3, July 1978, pp. 549-557.

24. D.H. Hibner, P.N. Bansal, and D.F. Buono, 'Analysis and Experimental Investigation of the Stability of Intershaft Squeeze Film Dampers - Part 2: Control of Instability', Journ. of Mech. Design, Vol. 100, No. 3, July 1978, pp. 558-562.

25. E.J. Hahn, 'Unbalance Behavior of Squeeze Film Supported Rigid Rotors'. Journ. of Mech. Design, Vol. 100, No. 3, July 1978, pp. 176-188.

26. J. M. Vance, 'A Current Review of Rotordynamics Problems in High Speed Lightweight Turbomachinery and Power Shafting', Proc. of the Conference on the Stability and Dynamic Response of Rotors with Squeeze Film Bearings, University of Virginia Charlottesville, May 1979, pp. 7-19.

27. D.H. Hibner and P.N. Bansal, 'Effects of Fluid Compressibility on Viscous Damper Characteristics', Proc. of the Conference on the Stability and Dynamic Response of Rotors with Squeeze Film Bearings', University of Virginia, Charlottesville, May 1979, pp. 116-132.

28. R. Holmes, 'The Control of Rotor Vibration Using Squeeze Film Dampers', Proc. of the Conference on the Stability and Dynamic Response of Rotors with Squeeze Film Bearings', University of Virginia, Charlottesville, May 1979, pp. 53-72

29. R.A. Cookson and S.S. Kossa, 'The Effectiveness of Squeeze-Film Damper Bearings Supporting Flexible Rotors without a Centralizing Spring', Int. J. Mech. Sci., Vol. 22, May 1980, pp. 313-324.

30. R.A. Cookson and S.S. Kossa, 'The Vibration Isolating Properties of Uncentralized Squeeze-Film Damper Bearings Supporting a Flexible Rotor', ASME International Gas Turbine Conference, Houston, Texas, March 1981.

31. R.D. Quinn, 'Experimental Study of Uncentralized Squeeze Film Dampers', M.S. Thesis, The University of Akron, Akron, Ohio, January 1984, 117 p.

NOMENCLATURE

C = radial clearance of damper annulus

D = nominal damper annulus diameter = $2R$

e = damper eccentricity

F_x = X - component of damper force

F_y = Y - component of damper force

h = damper annulus film thickness distribution

L = damper length

p = damper film thickness distribution

R = nominal damper annulus radius

t = time

x = $R\theta$ = damper annulus circumferential coordinate

X = X - direction radial motion coordinate

Y = Y - direction radial motion coordinate

z = damper annulus axial coordinate

μ = damper lubricant viscosity

Ω = frequency of vibration excitation

SPECIAL TERMINOLOGY

Infinitely Long Bearing Model - axial flow is neglected $(\frac{\partial}{\partial z} << \frac{\partial}{\partial x})$

Infinitely Short Bearing Model - circumferential flow is neglected $(\frac{\partial}{\partial x} << \frac{\partial}{\partial z})$

Driver Code - Any computer code which calls the squeeze-film damper force computation code

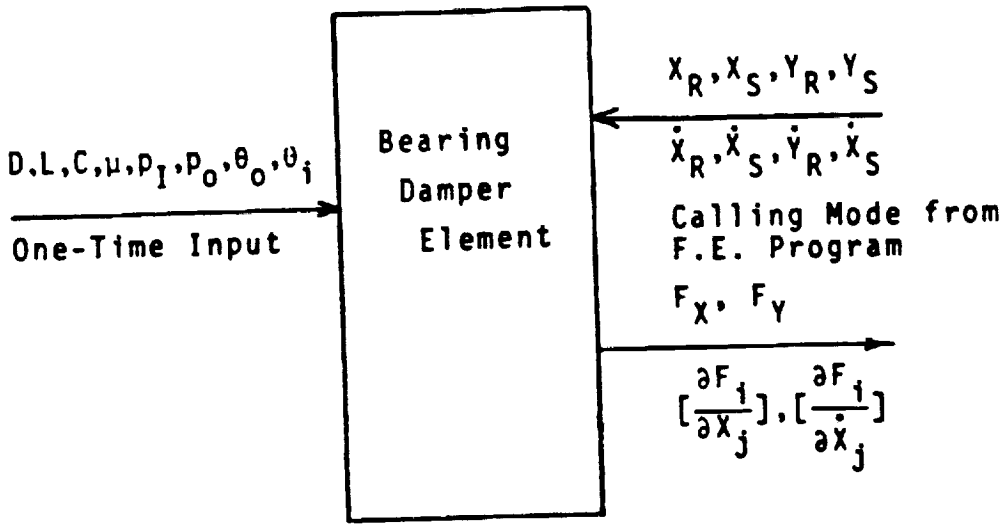

Fig.1 Input/Output of Damper Pilot Code

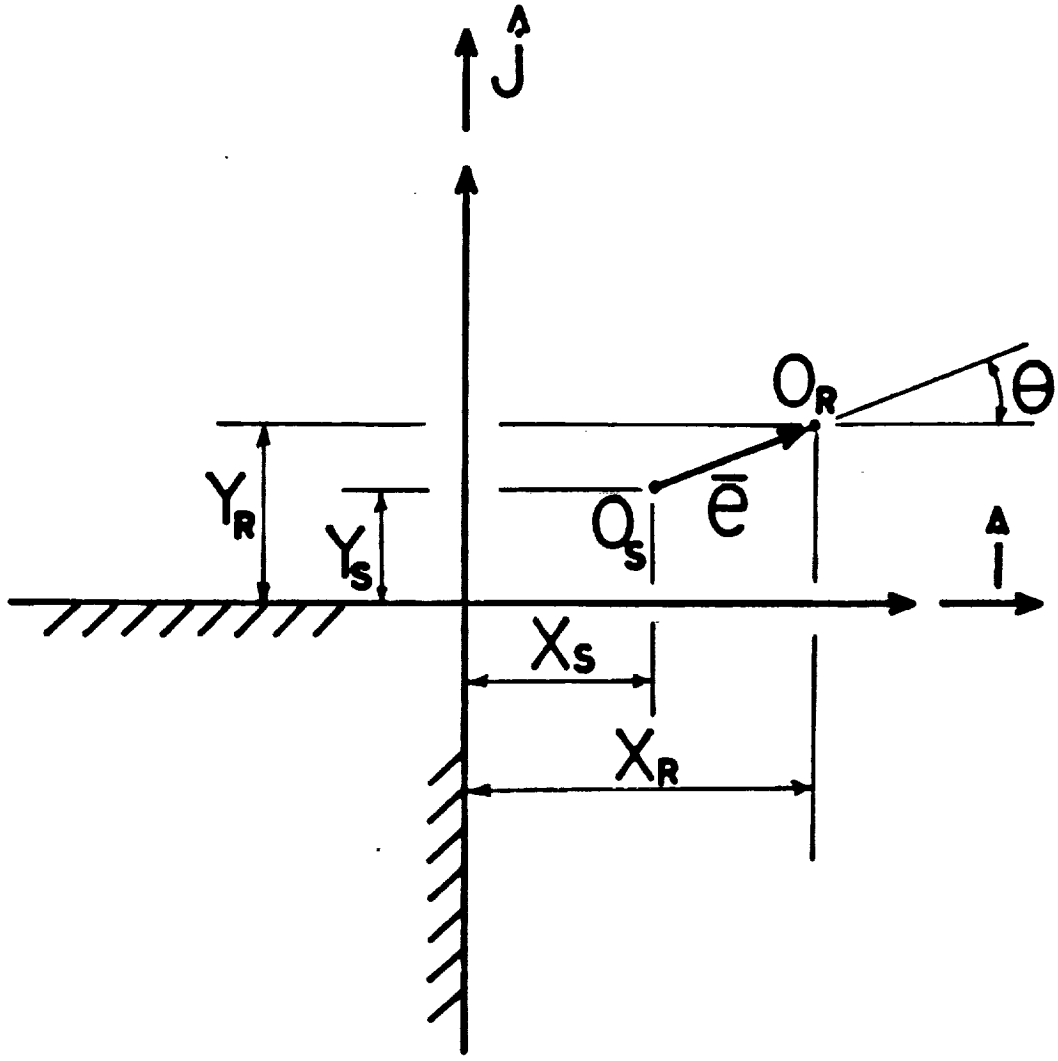

Fig. 2 Inertial coordinates

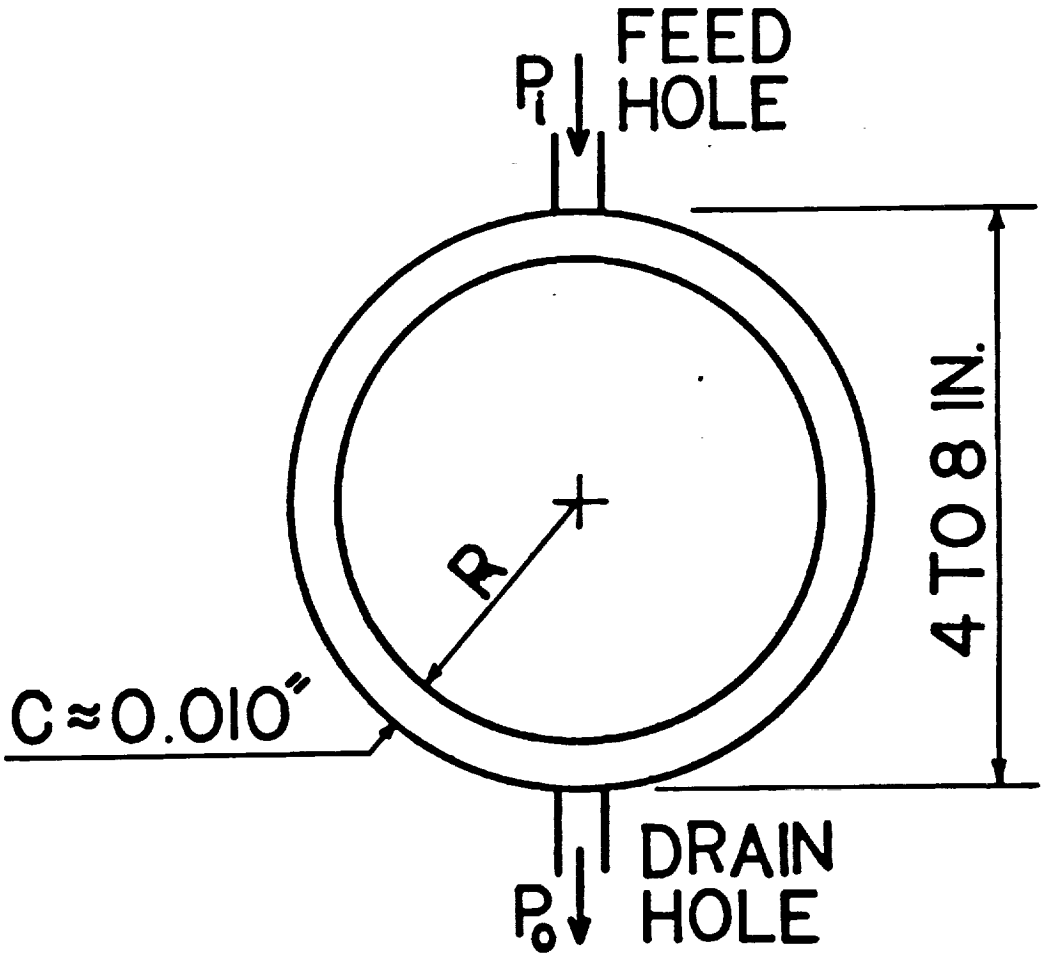

Fig. 3 A typical aircraft engine damper configuration

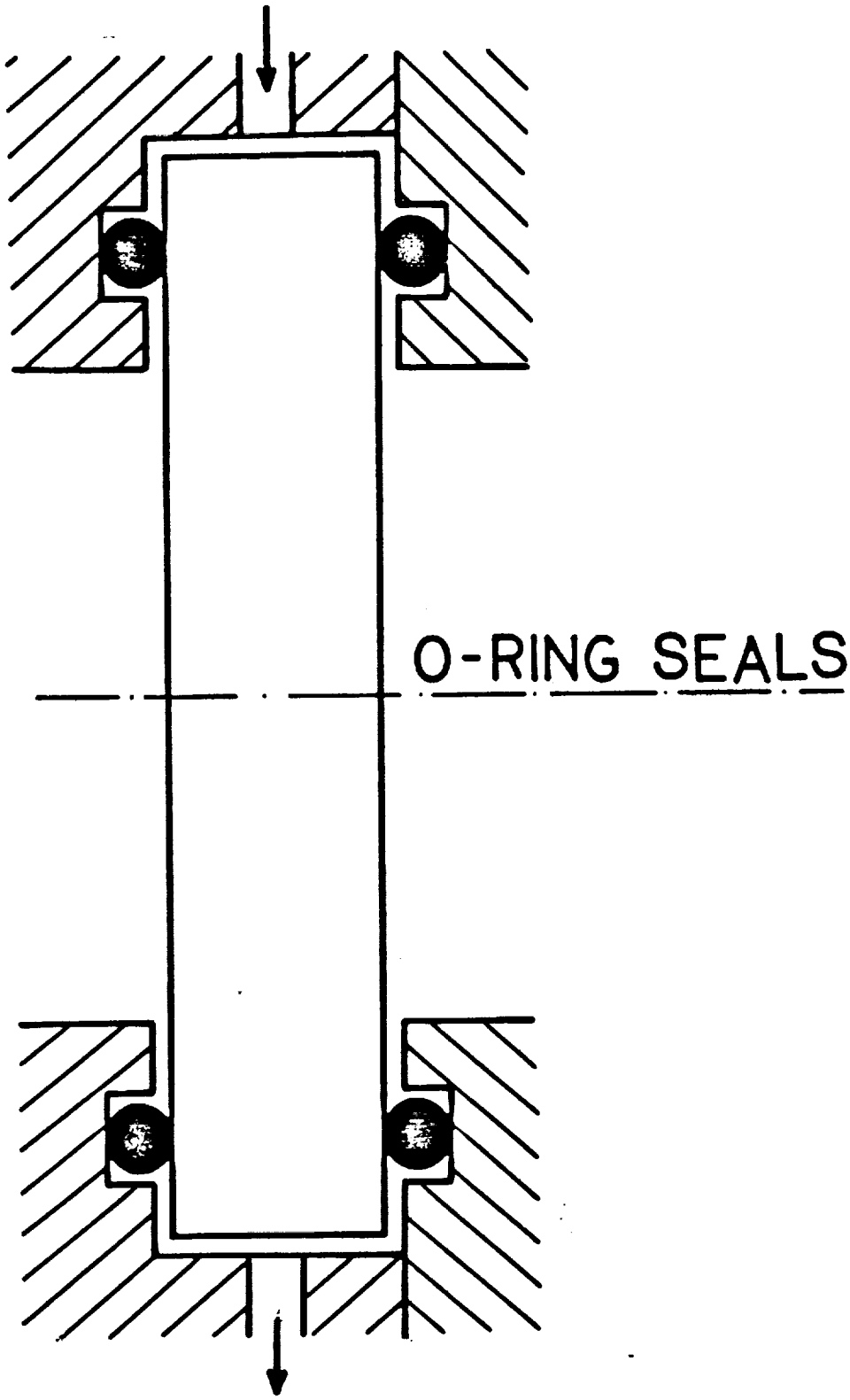

Fig. 4(a) Configuration frequently used in military applications

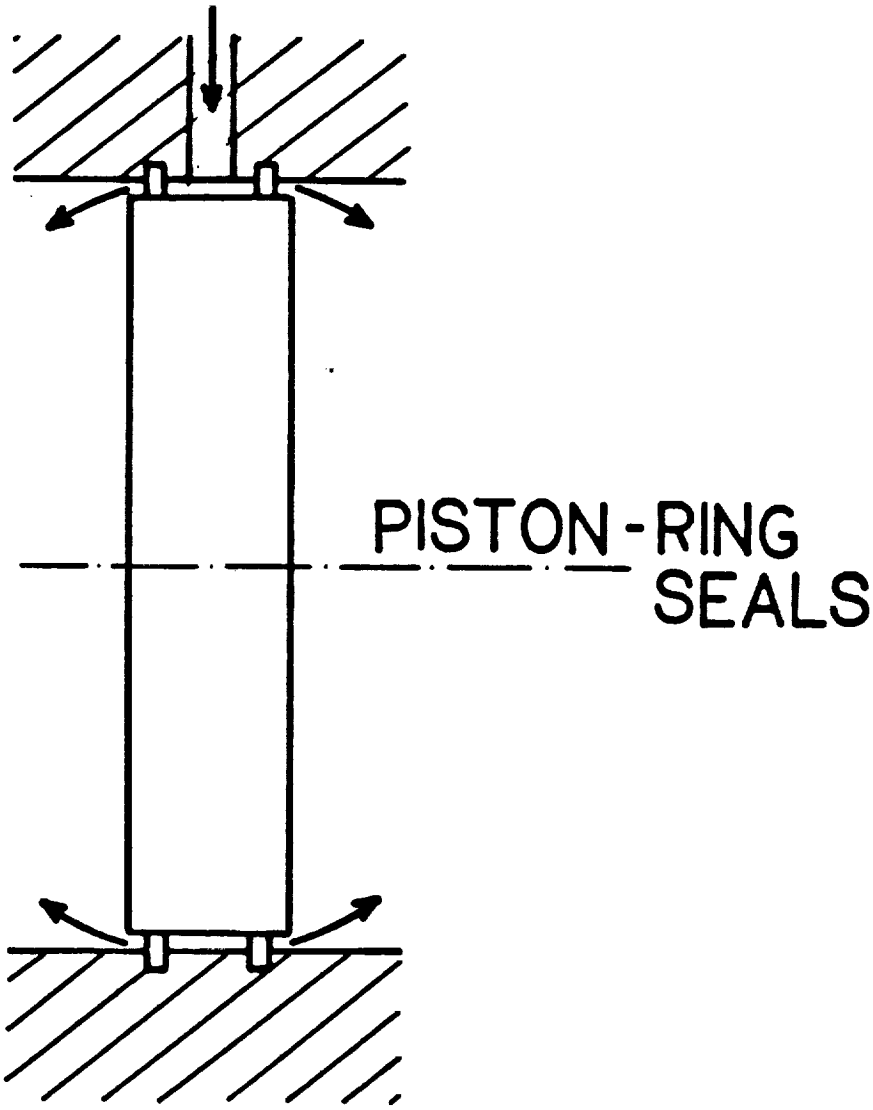

Fig. 4(b) Configuration frequently used in commercial applications

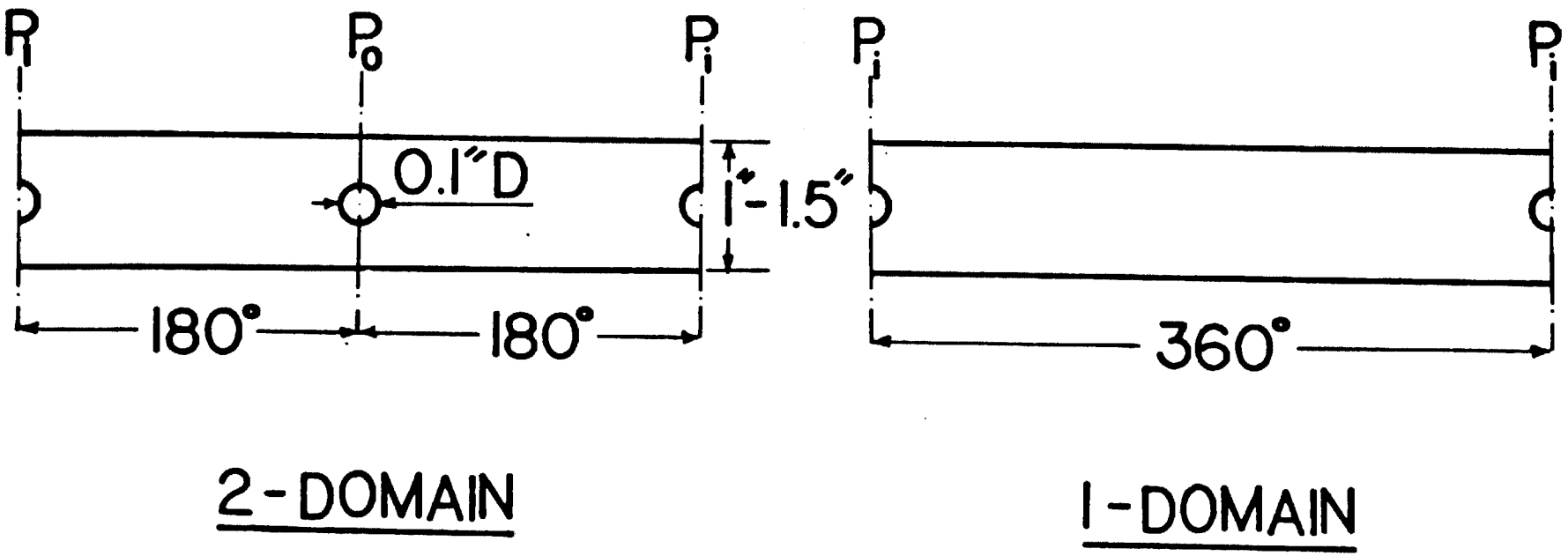

Fig. 5 Unwrapped squeeze-film pressure solution domains for configurations shown in Figure 4.

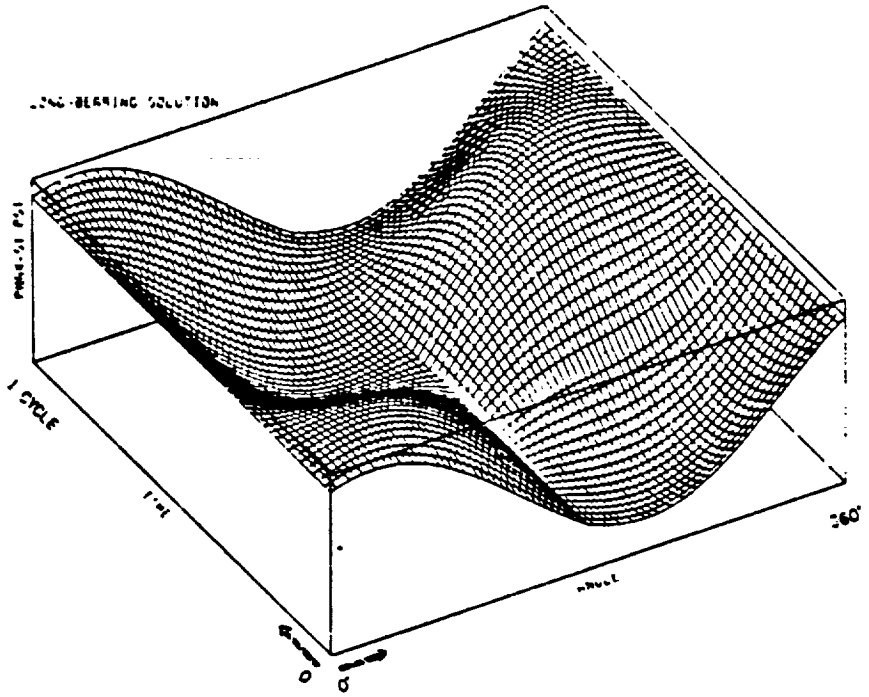

(a) e/c=0.05

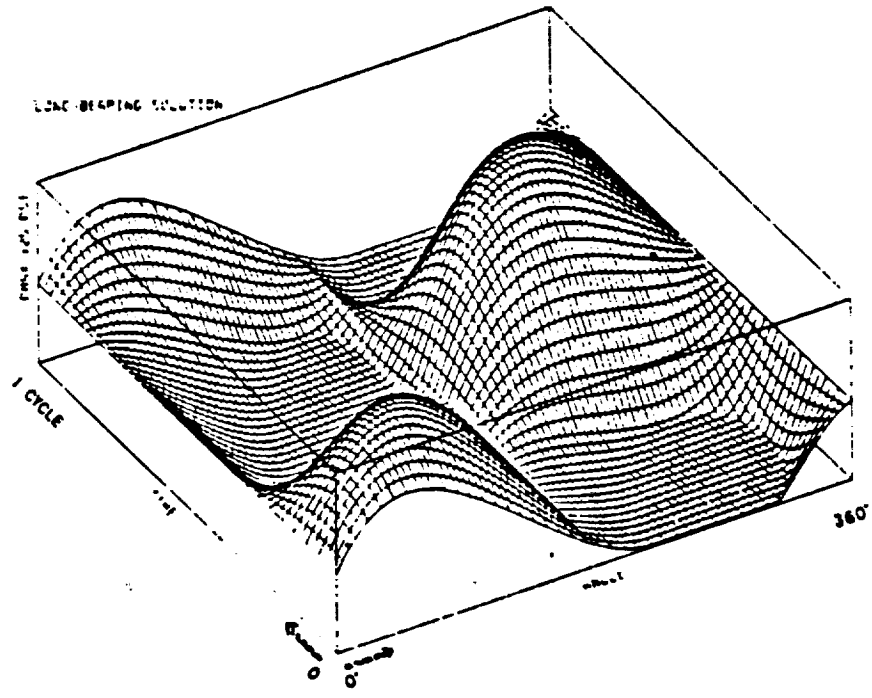

(b) e/c=0.20

Figure 6 Pressure distribution in circumferential direction and time of one cycle of circular orbit(long-bearing solution).

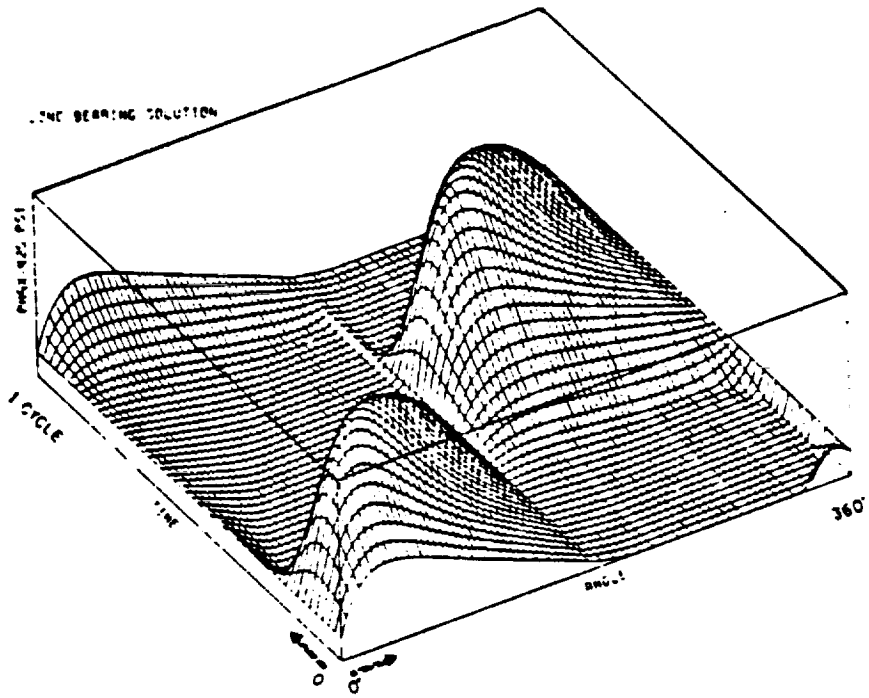

(c) e/c=0.60

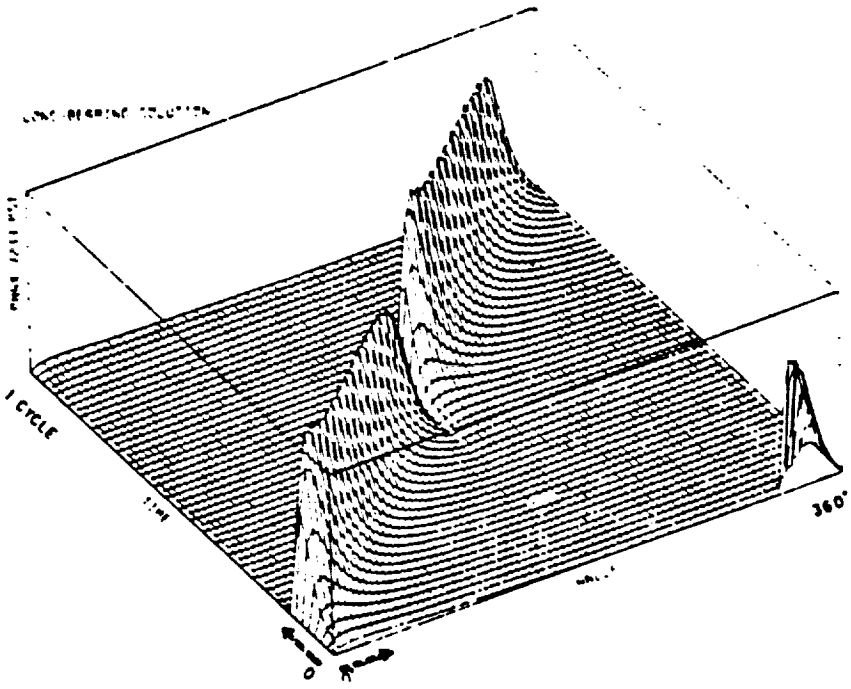

(d) e/c=0.95

Figure 6 Pressure distribution in circumferential direction and time (Cont'd) of one cycle of circular orbit (long-bearing solution).

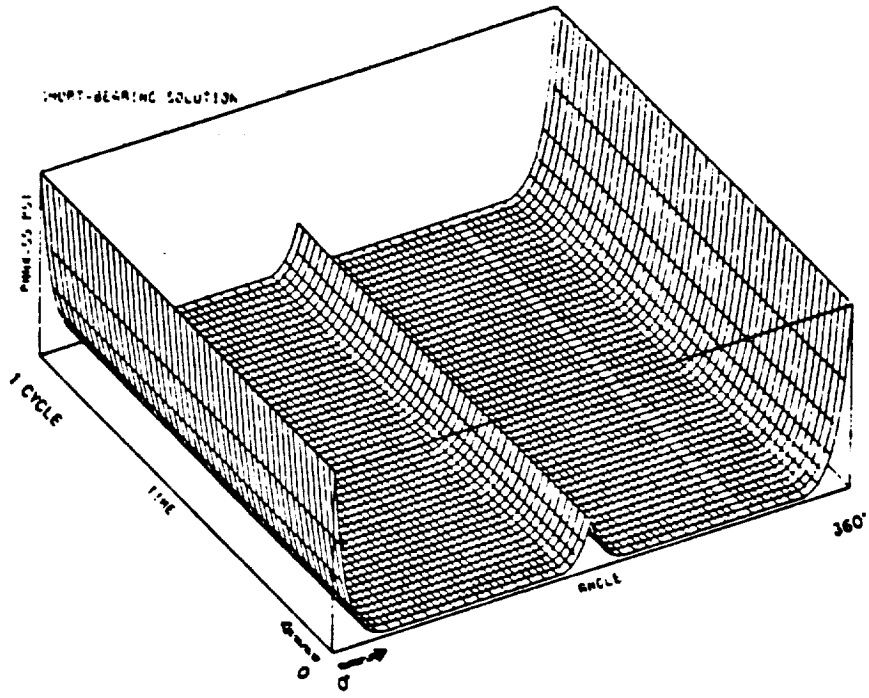

(a) e/c=0.05

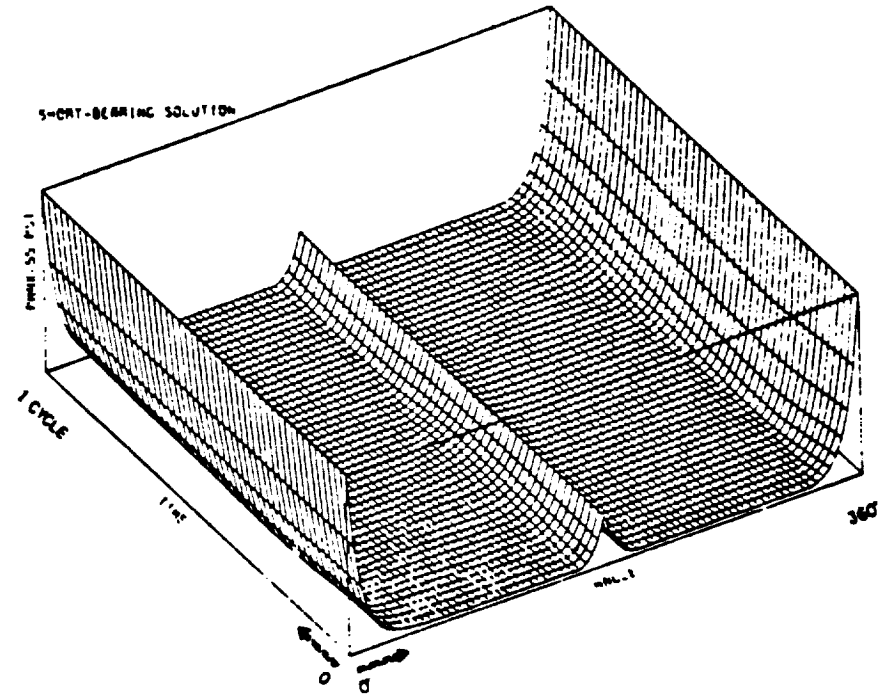

(b) e/c=0.20

Figure 7 Pressure distribution in circumferential direction and time of one cycle of circular orbit (short-bearing solution).

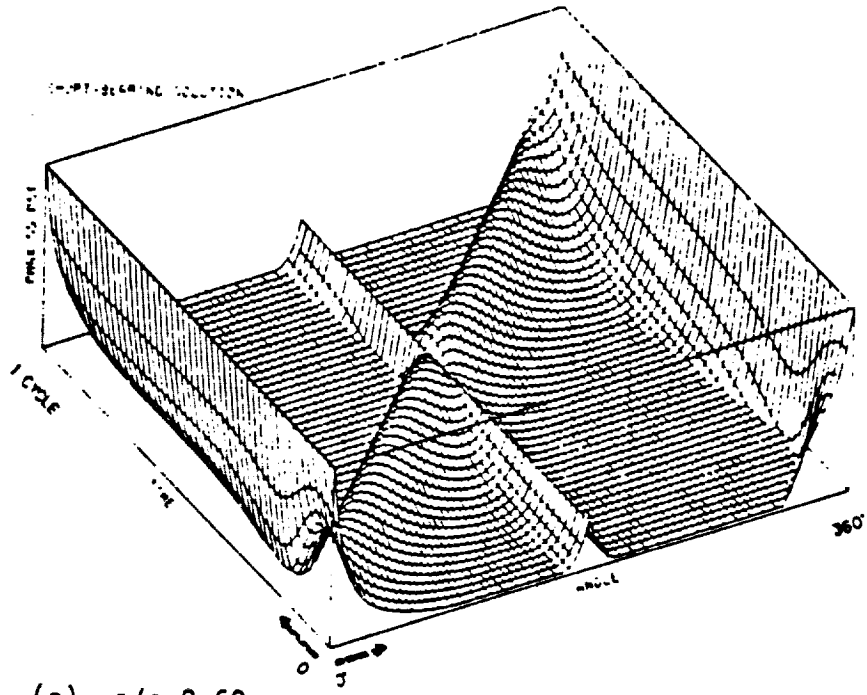

(c) e/c=0.60

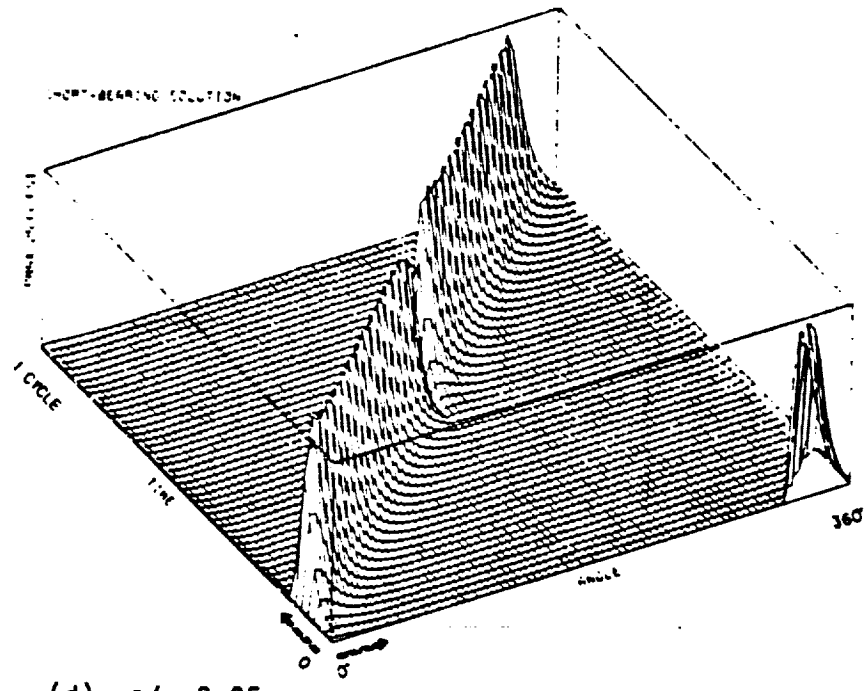

(d) e/c=0.95

Figure 7 Pressure distribution in circumferential direction and time (Cont'd) of one cycle of circular orbit (short-bearing solution).

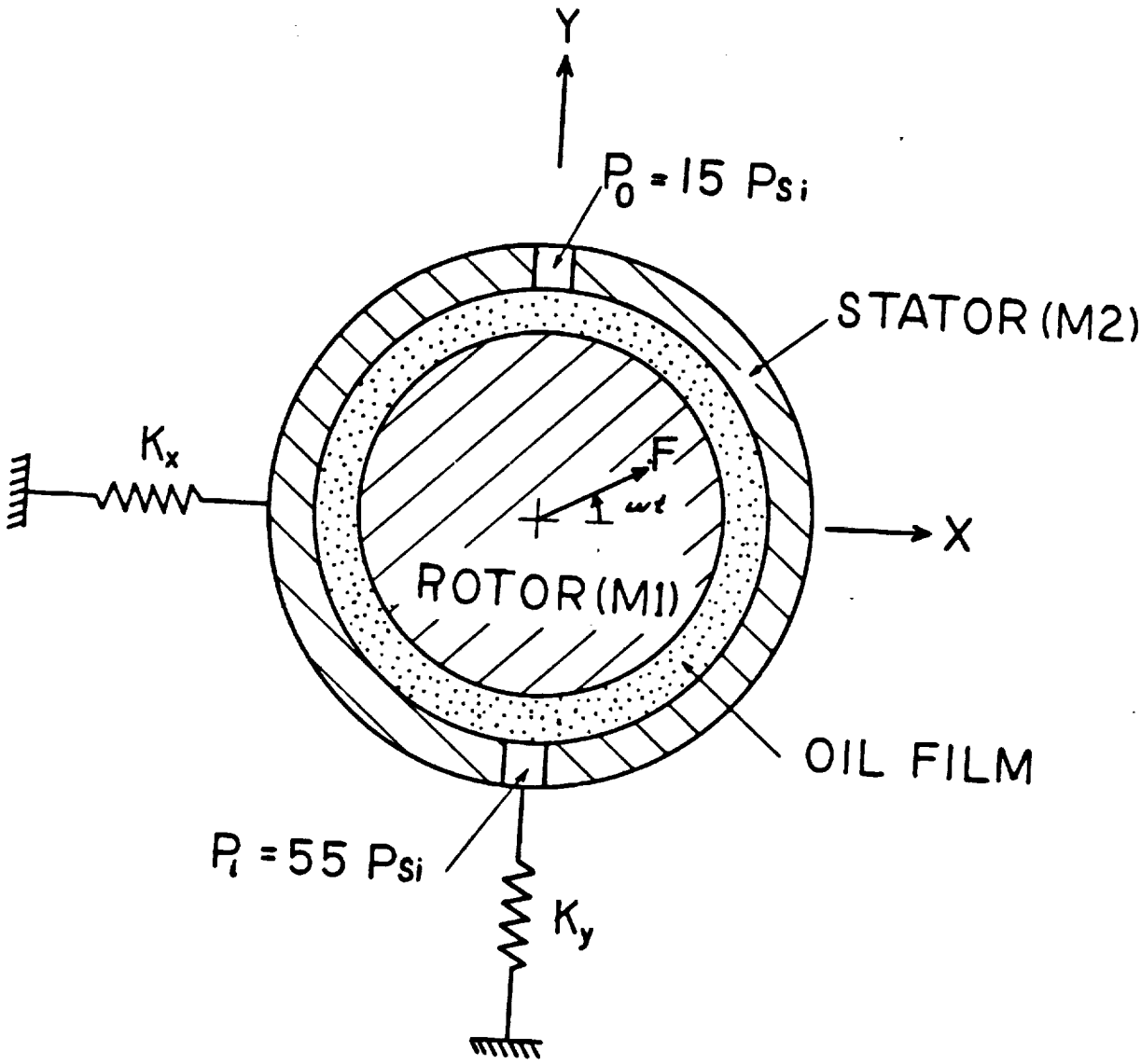

Figure 8 Simple 2-mass,4-degree of freedom. Test case (Same damper parameters as on page 18)

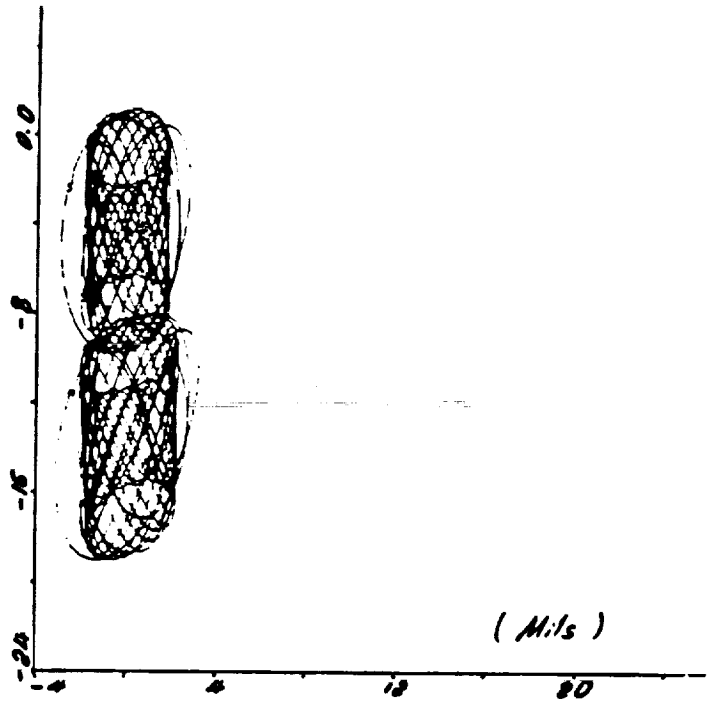

(a) Rotor and stator orbits

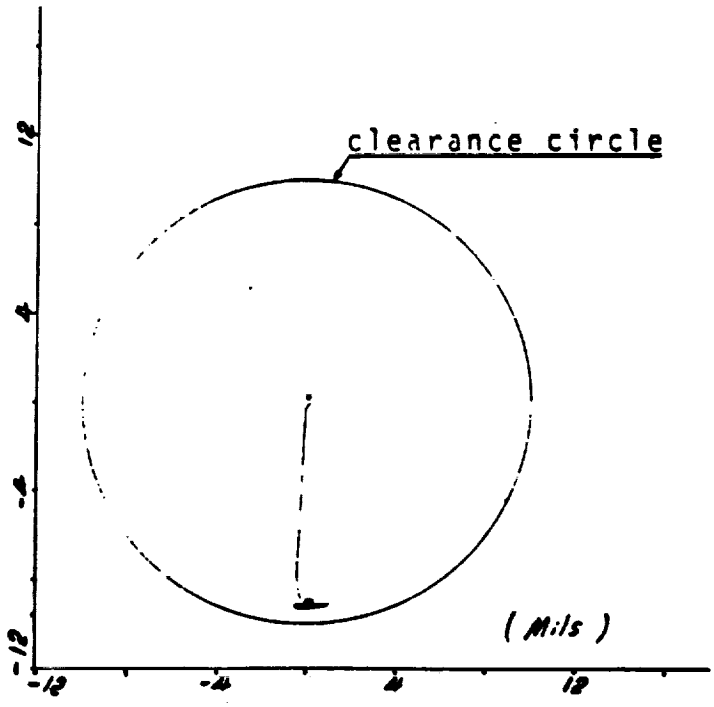

(b) Rotor orbit relative to stator (clearance circle shown)

Fig.9 Nonlinear dynamic transient of simple 4 DOE system(See Fig.8) $|F|$=100 lbs, ω=150 rad/sec, M1=M2=500 lbs, Kx=Ky=116000 lbs/in.

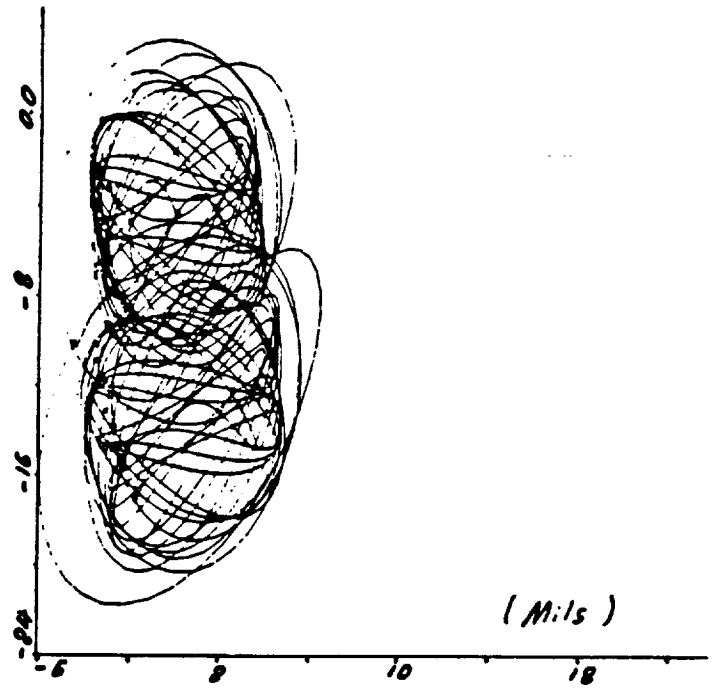

(a) Rotor and stator orbits

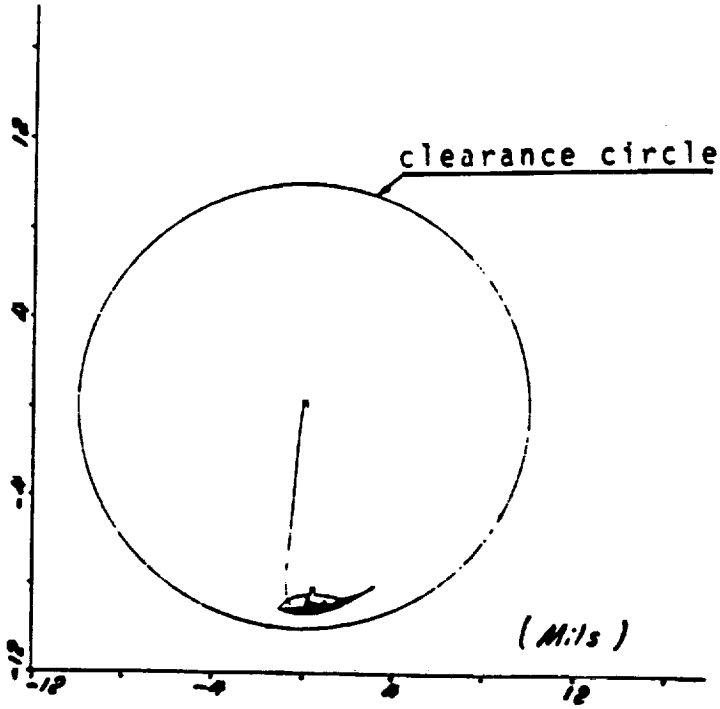

(b) Rotor orbit relative to stator (clearance circle shown)

Fig.10 Nonlinear dynamic transient of simple 4 DOE system(See Fig.8) $|F|$=200 lbs, ω=150 rad/sec, M1=M2=500 lbs, Kx=Ky=116000 lbs/in.

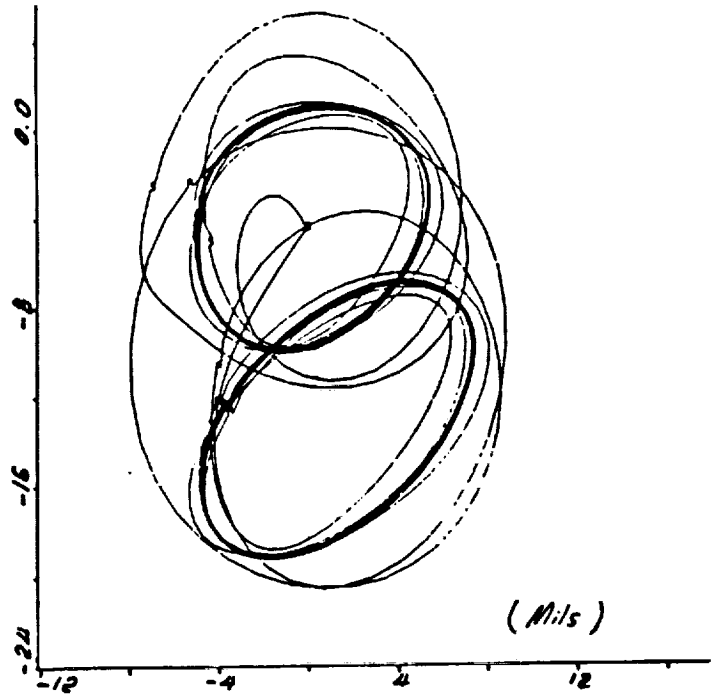

(a) Rotor and stator orbits

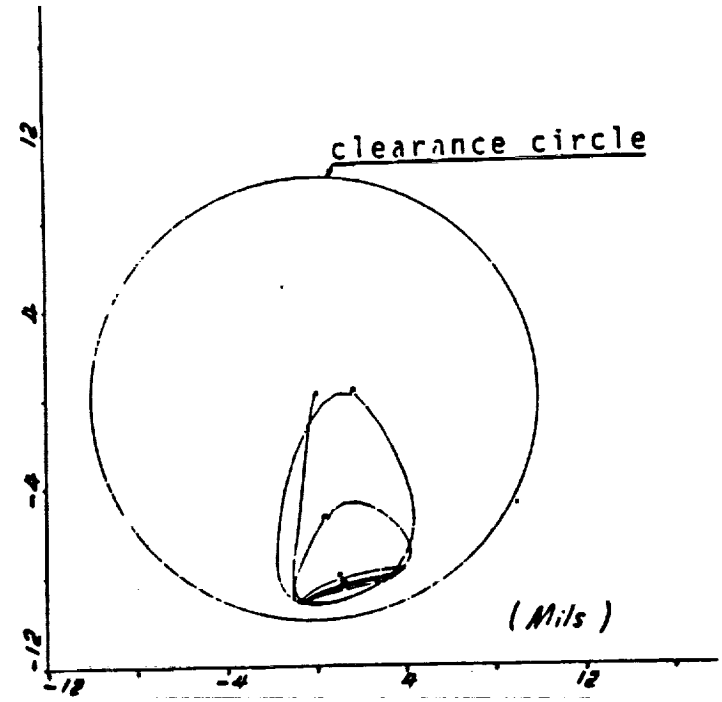

(b) Rotor orbit relative to stator (clearance circle shown)

Fig.11 Nonlinear dynamic transient of simple 4 DOE system(See Fig.8) $|F|$=300 lbs, ω=150 rad/sec, M1=M2=500 lbs, Kx=Ky=116000 lbs/in.

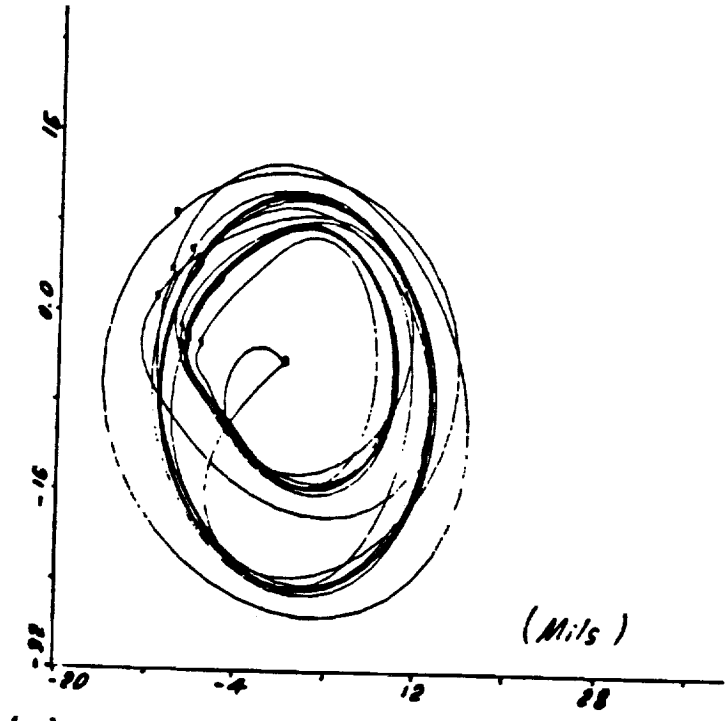

(a) Rotor and stator orbits

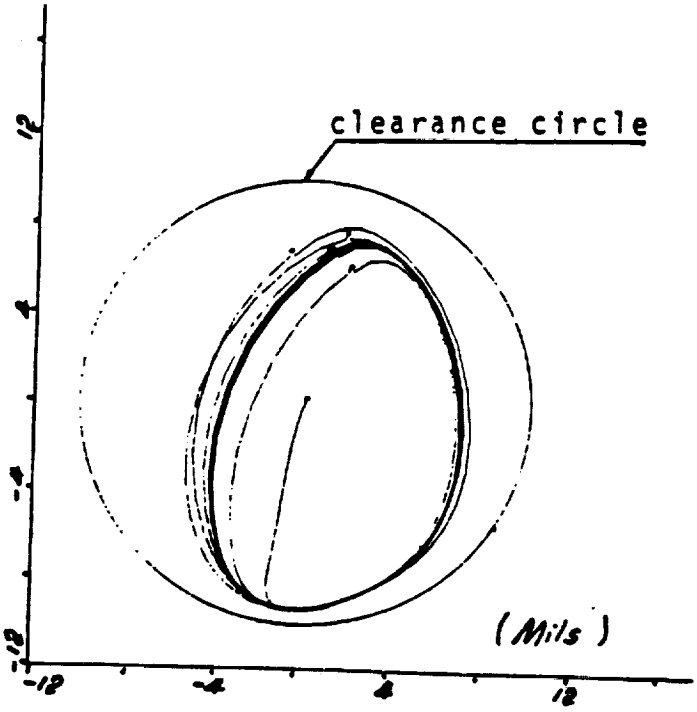

(b) Rotor orbit relative to stator (clearance circle shown)

Fig. 12 Nonlinear dynamic transient of simple 4 DOE system(See Fig.8) $|F|$=500 lbs, ω=150 rad/sec, M1=M2=500 lbs, Kx=Ky=116000 lbs/in.

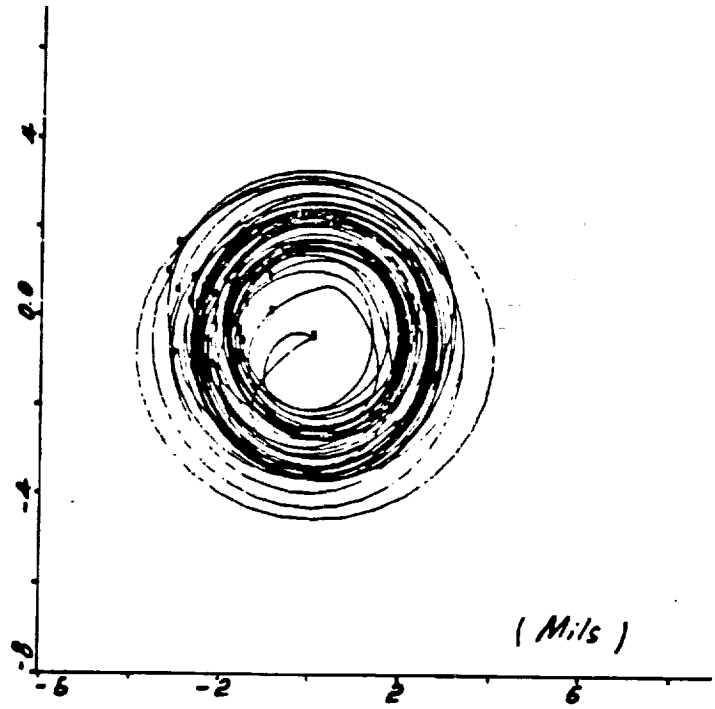

(a) Rotor and stator orbits

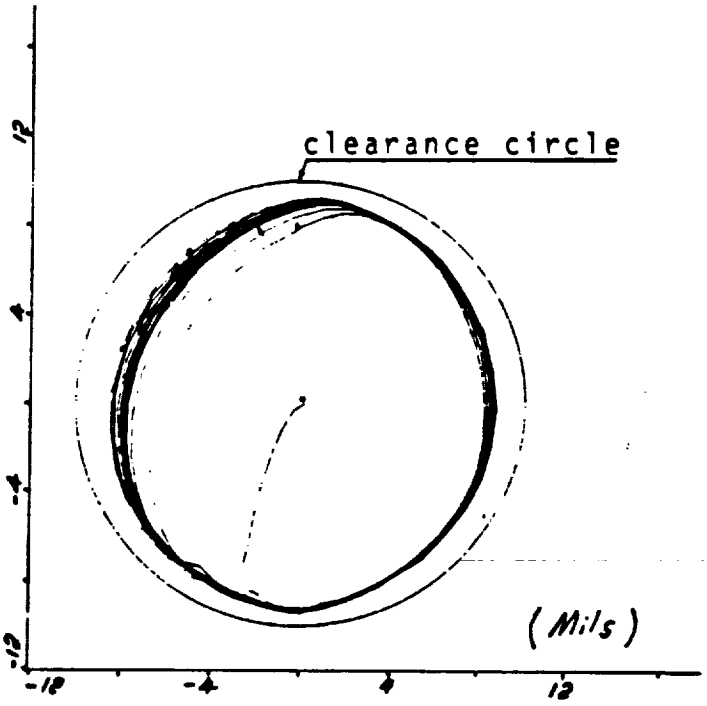

(b) Rotor orbit relative to stator
(clearance circle shown)

Fig.13 Nonlinear dynamic transient of simple 4 DOE system
$|F|$=1000 lbs, ω=150 rad/sec, M1=M2=500 lbs, Kx=Ky=116000 lbs/in

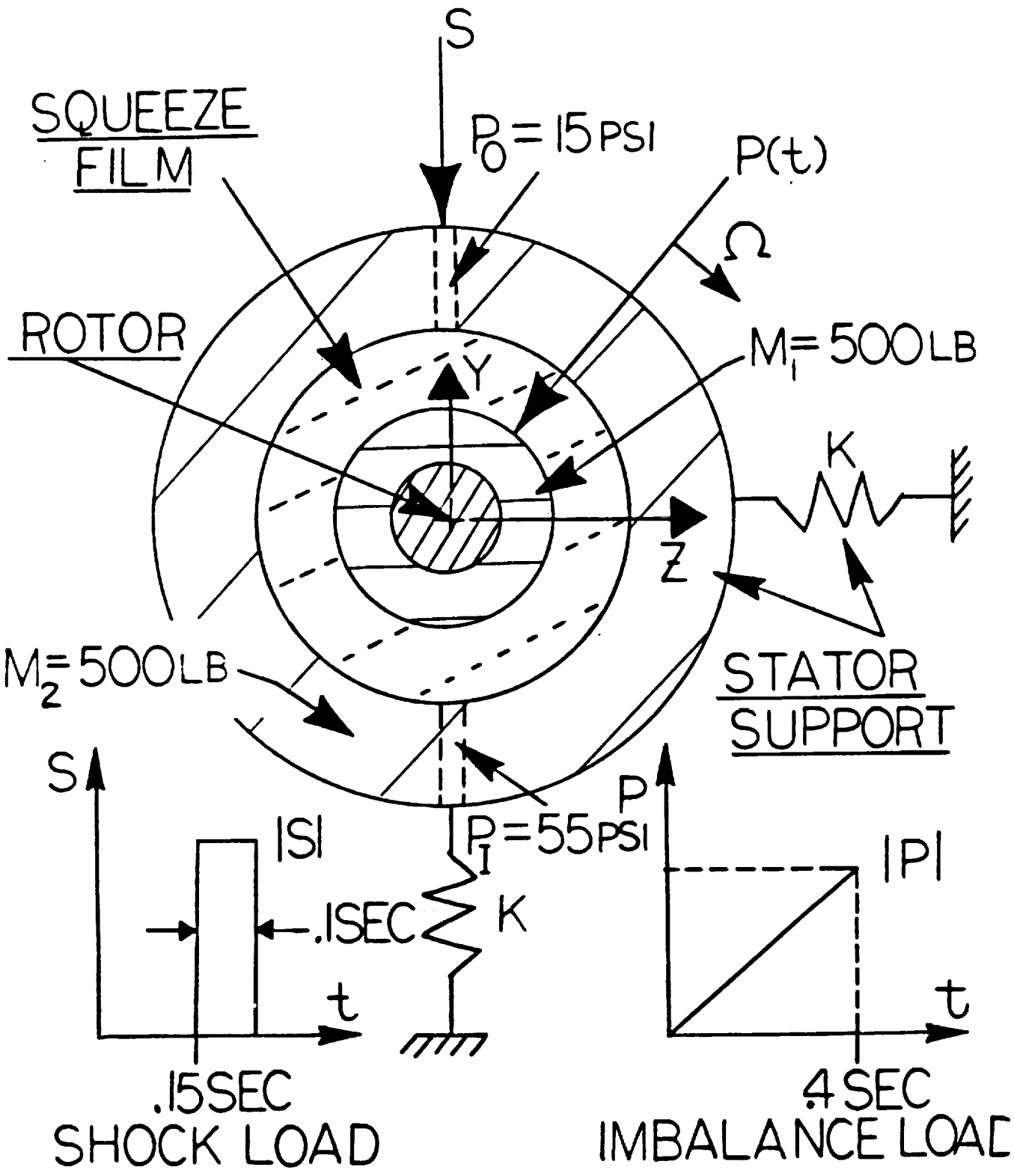

Fig. 14. Single Bearing Model

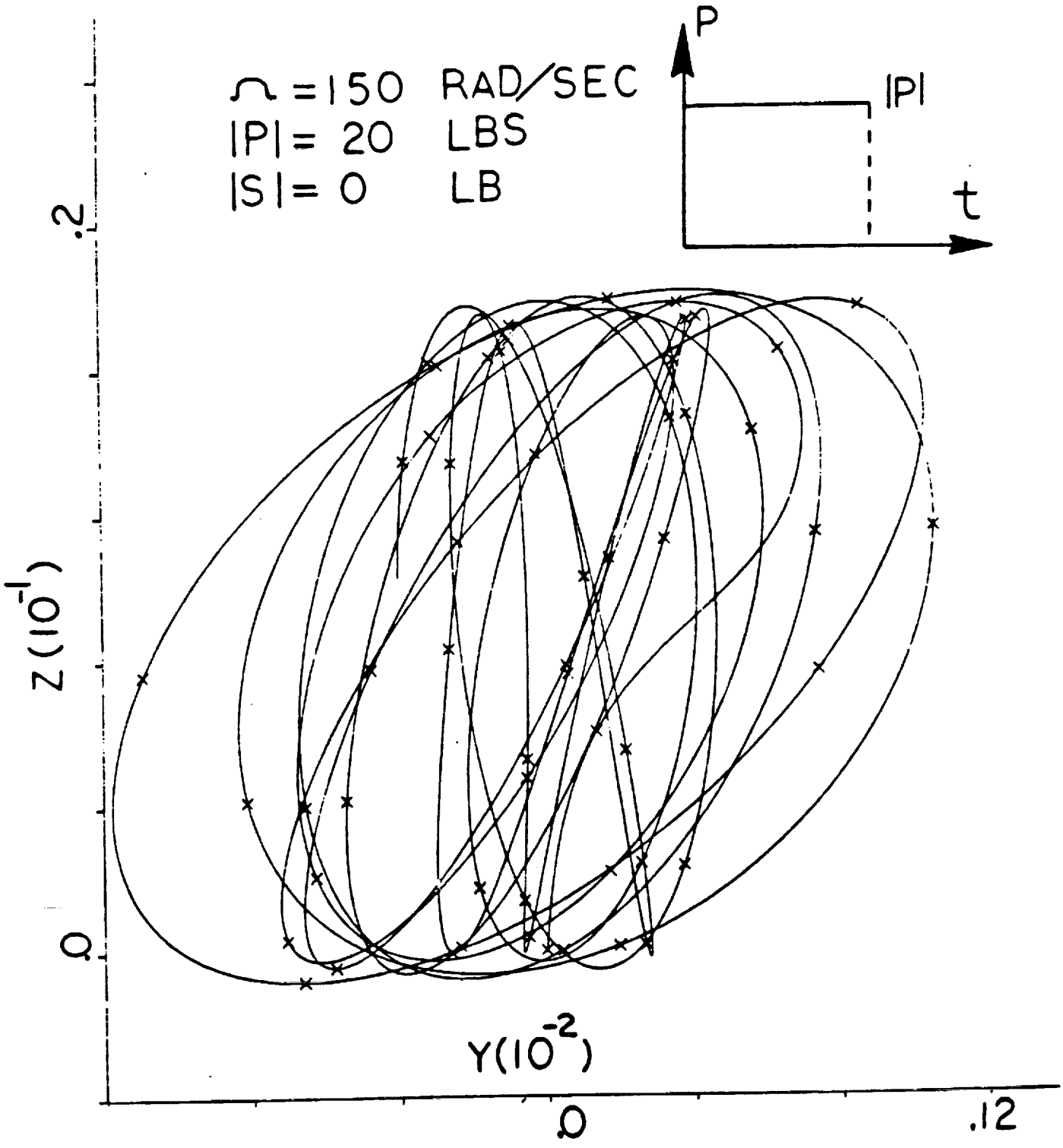

Fig. 15. Rotor Displacement;
|P| = 20 lbs.

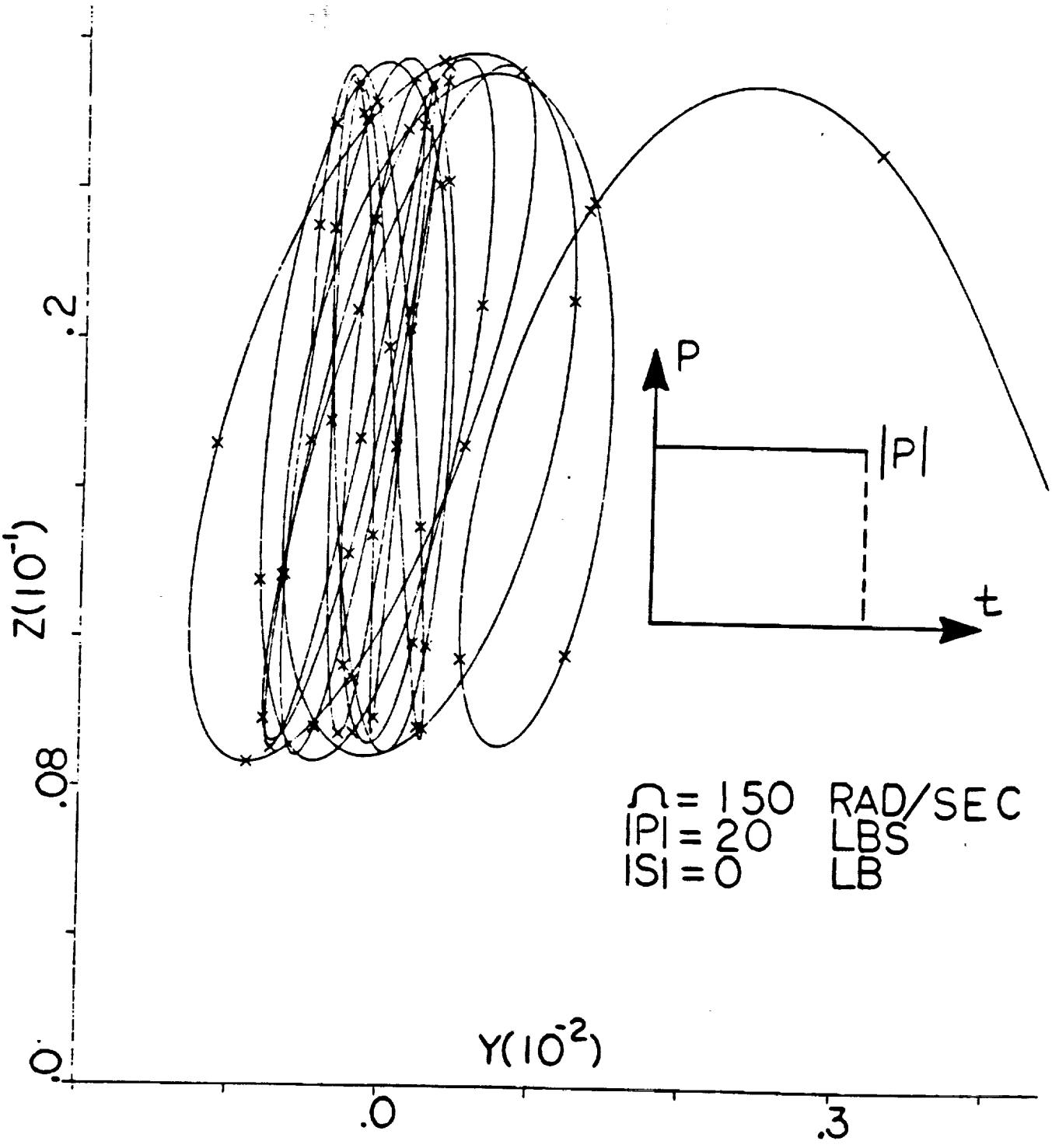

Fig. 16. Stator Displacement;
$|P|$ = 20 lbs.

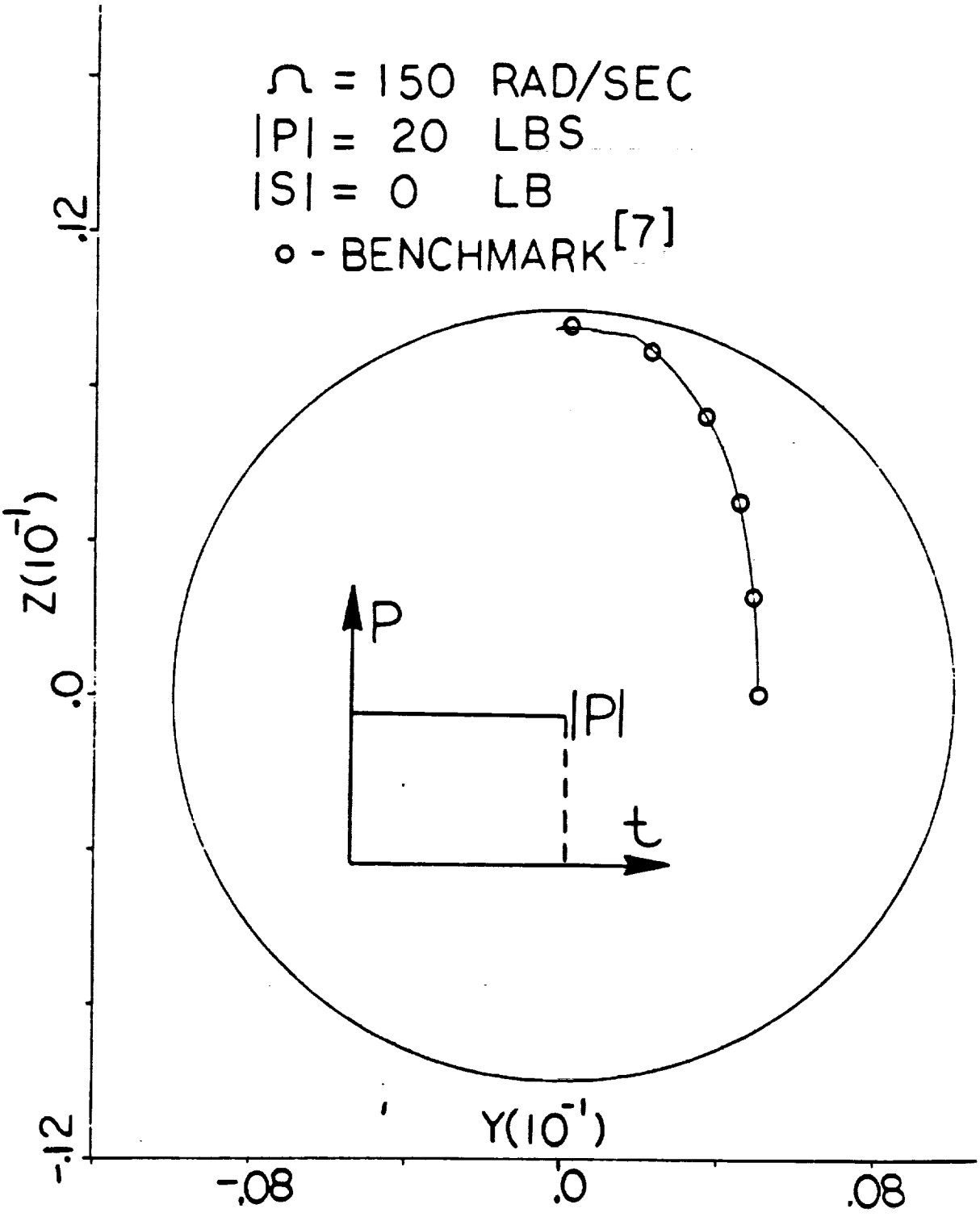

Fig. 17. Rotor Orbit; |P| = 20 lbs.

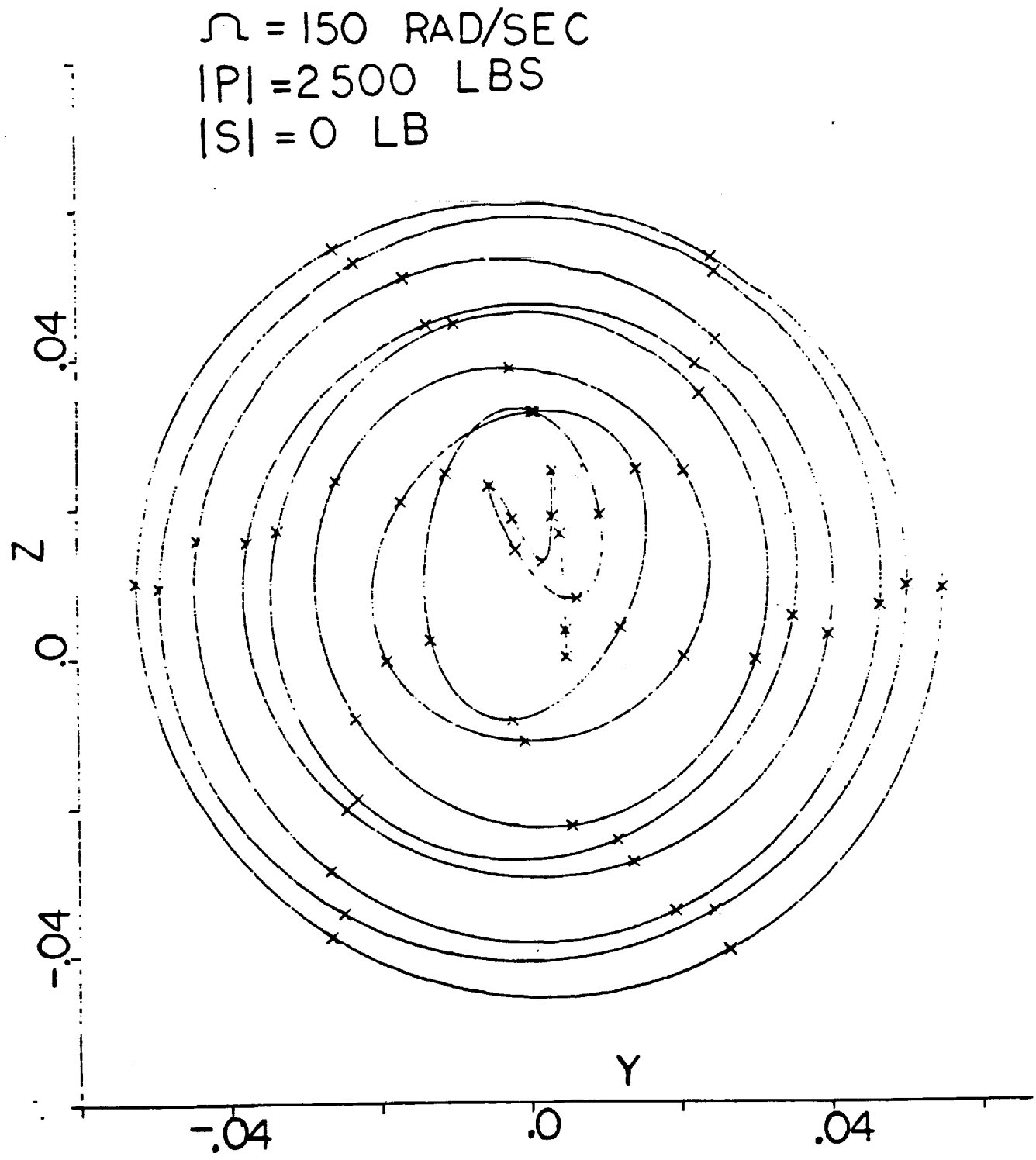

Fig. 18. Rotor Displacement; |P| = 2500 lbs.

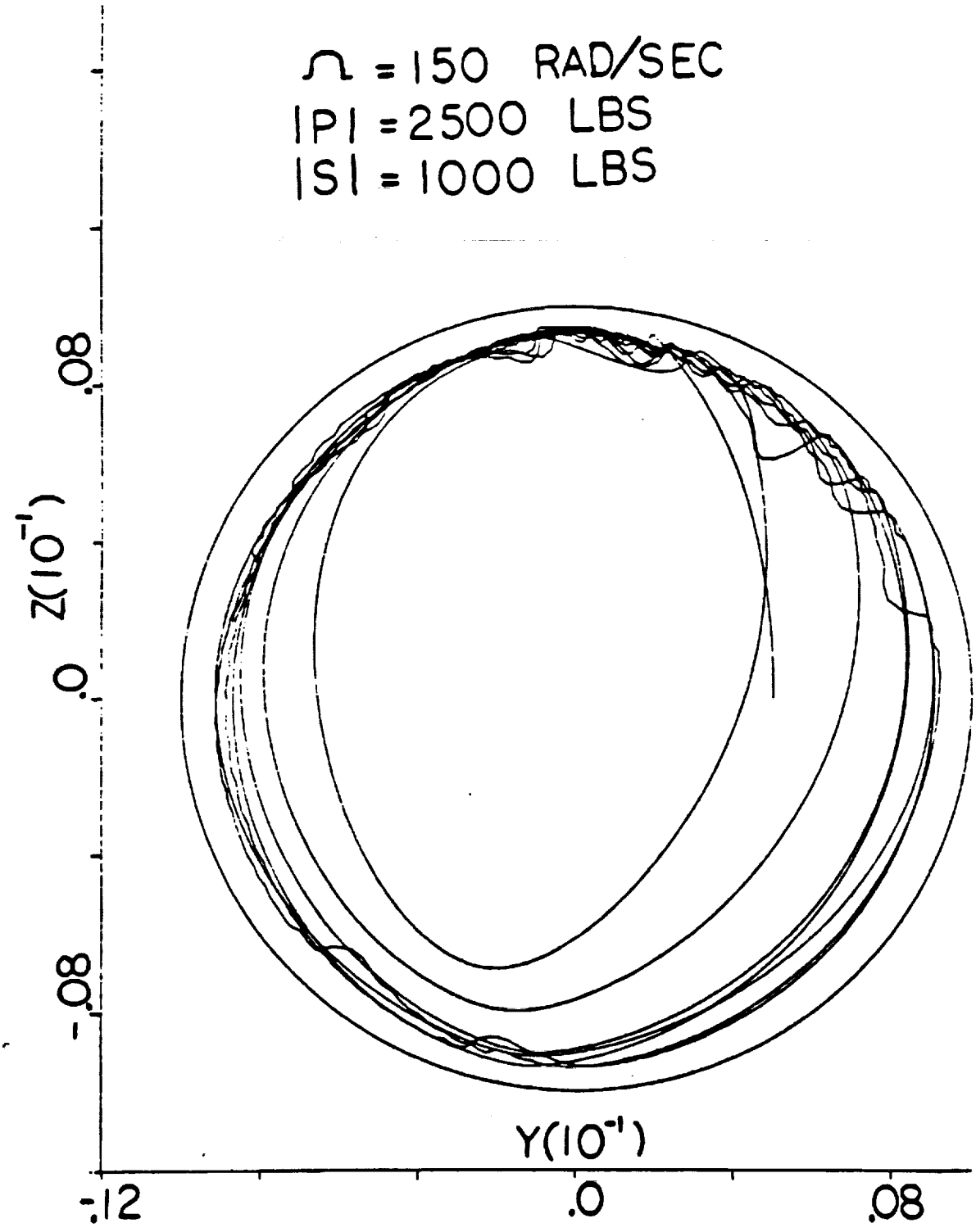

Fig. 19. Stator Displacement;
$|P|$ = 2500 lbs.

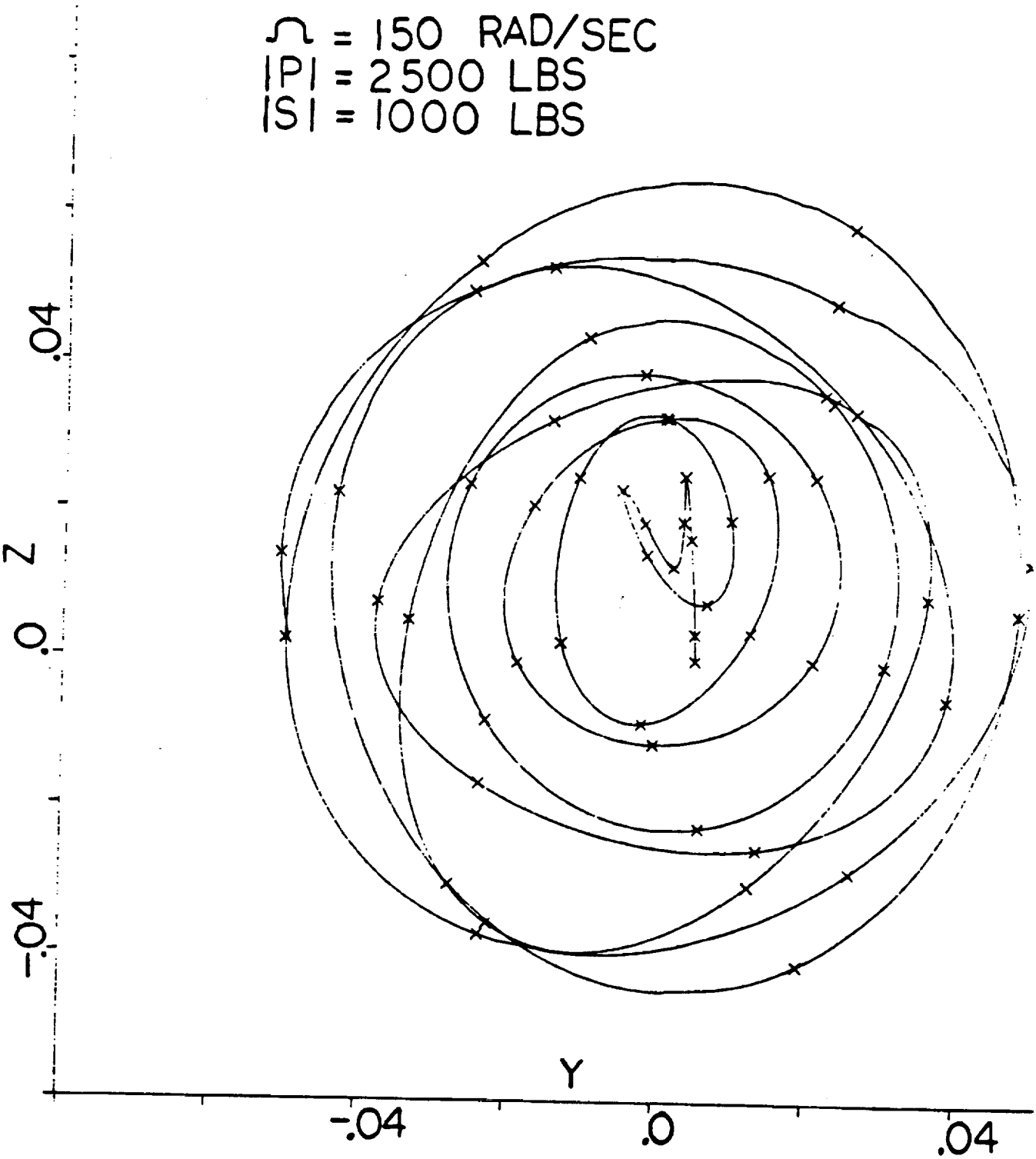

FIGURE 6.14 ROTOR DISPLACEMENT (SEE FIG. 6.1)

Fig. 20. Rotor Orbit; |P| = 2500 lbs.

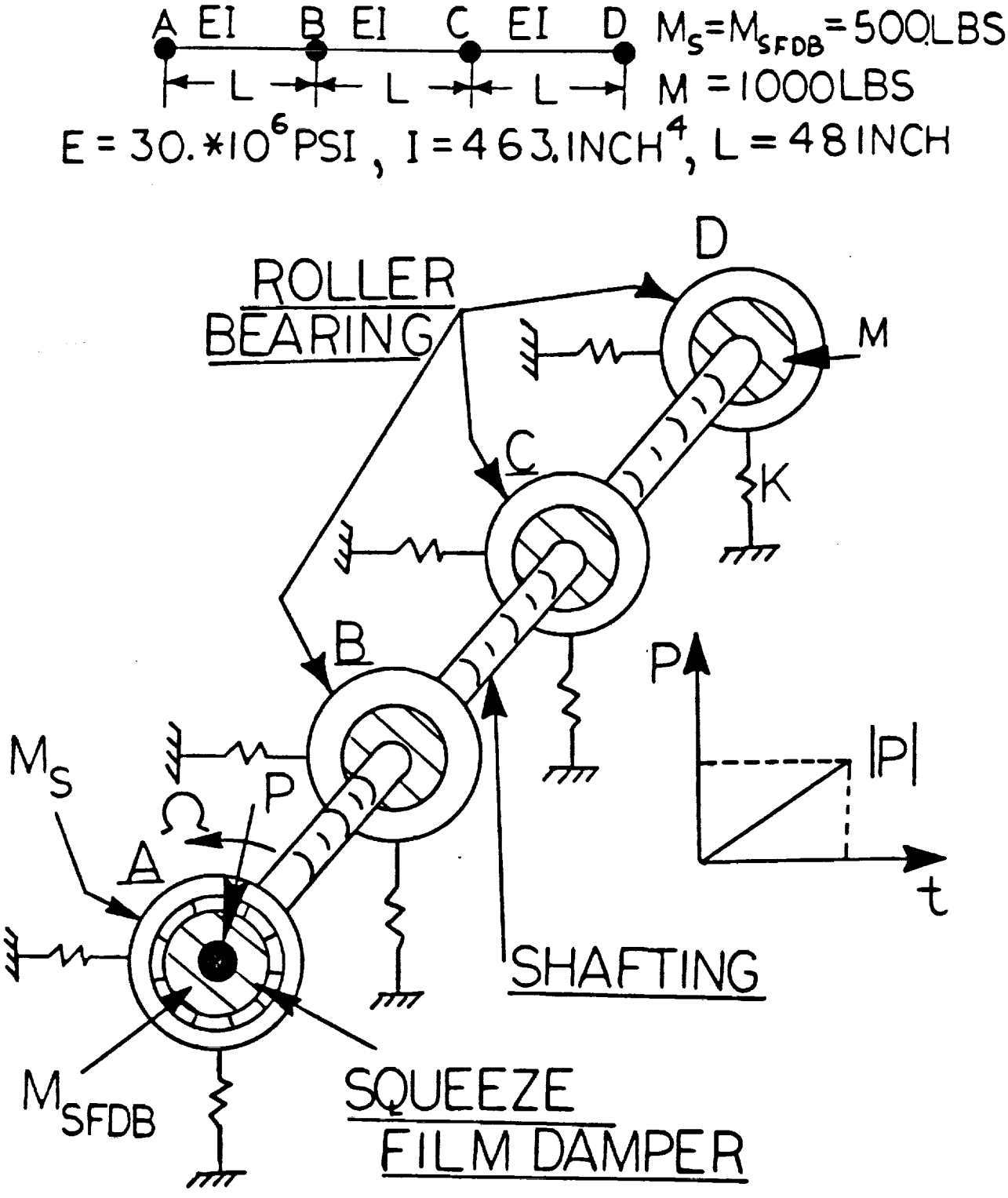

Fig. 21. Multibearing Model

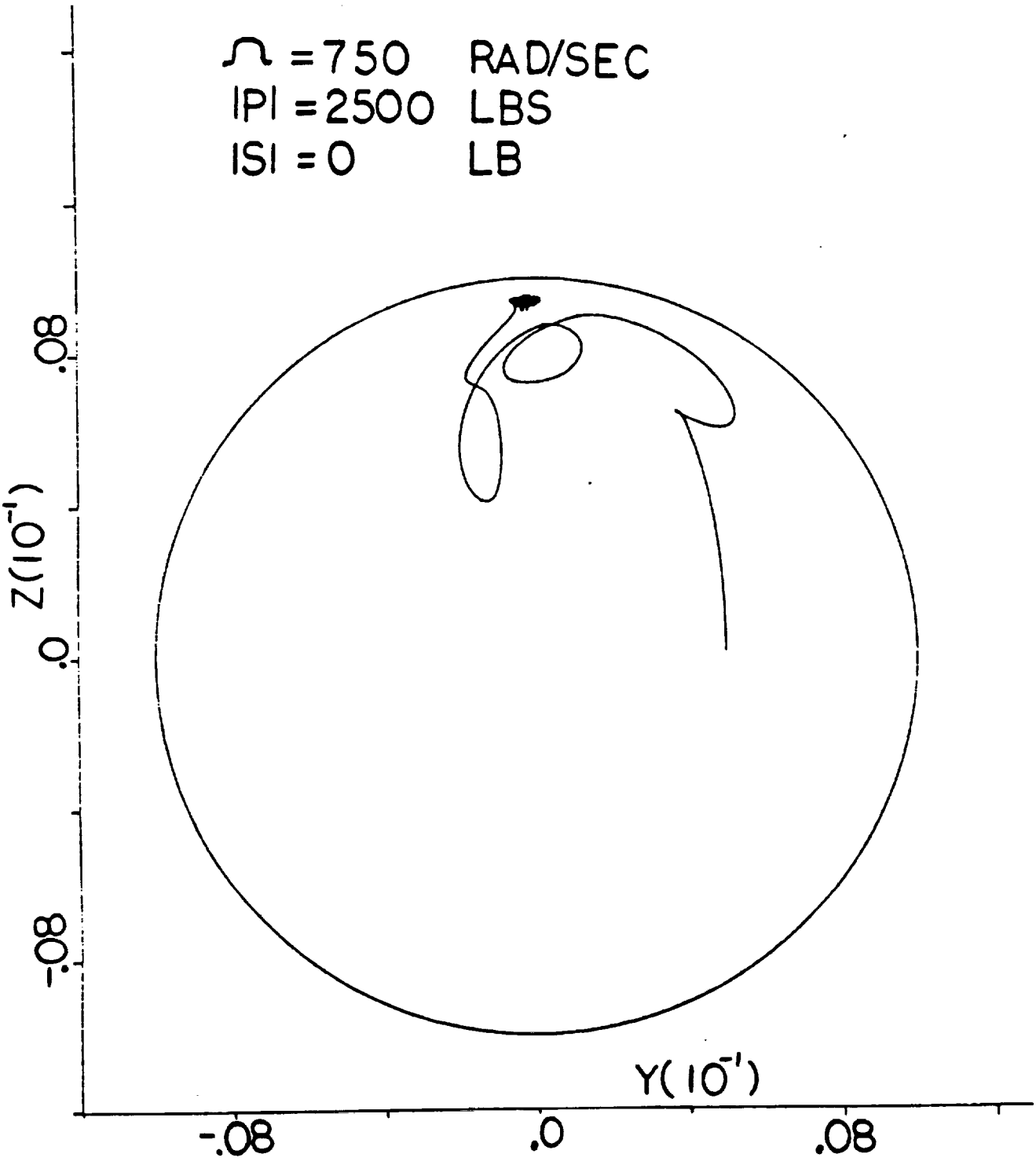

Fig. 22. Rotor Orbit;
$|P|$ = 500 lbs.

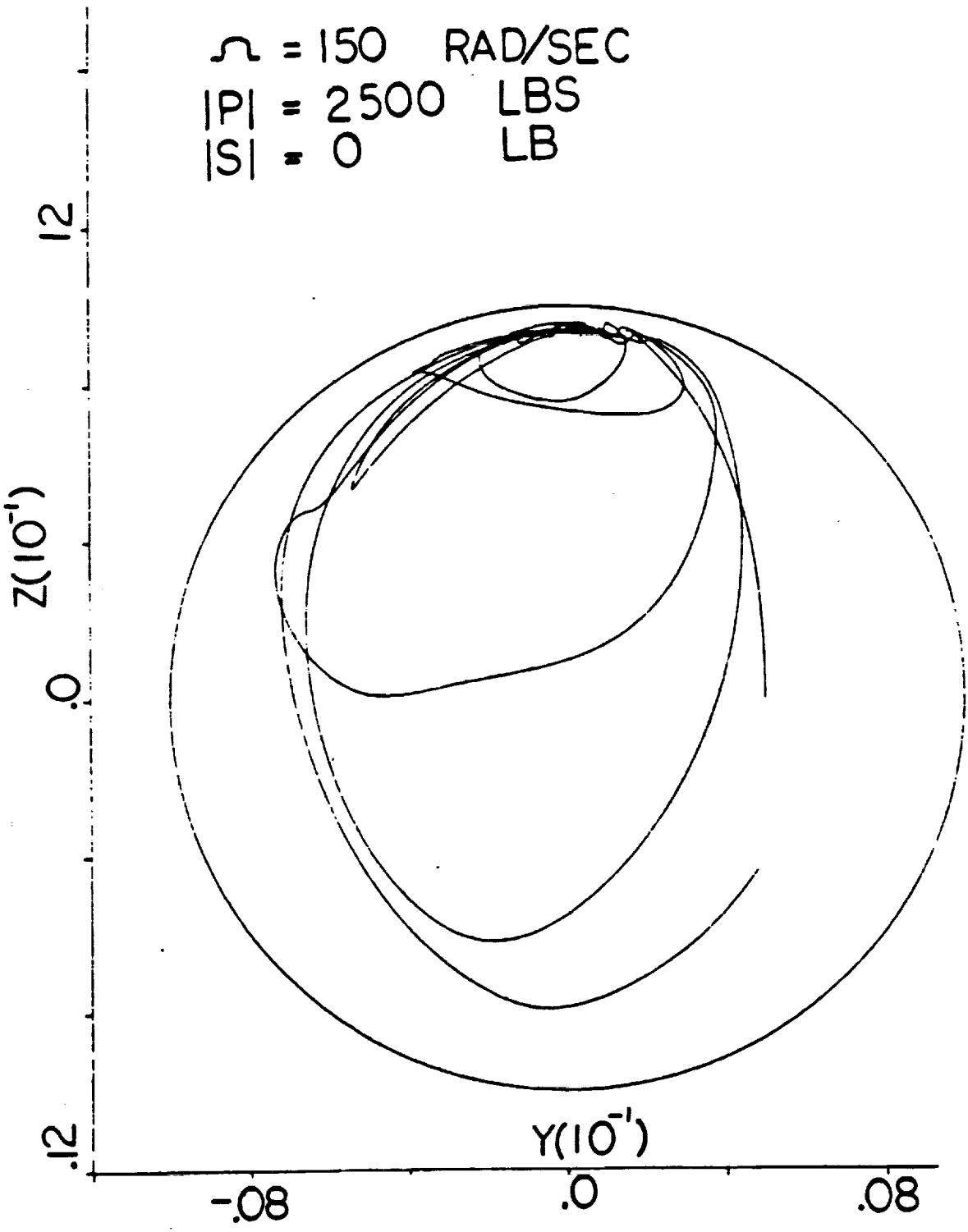

Fig. 23. Rotor Orbit;
|P| = 2500 lbs.

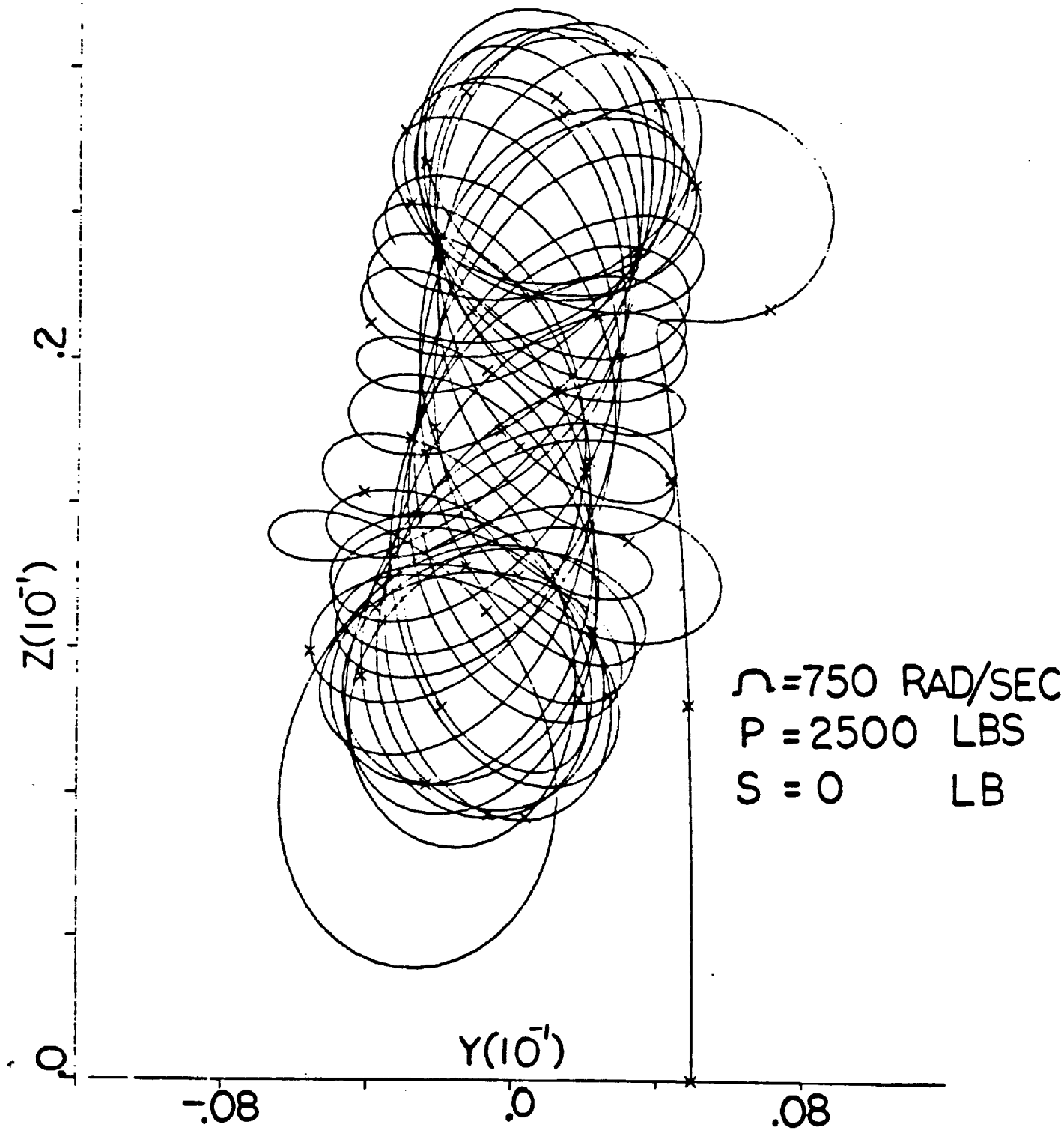

Fig. 24. Rotor Displacement;
$|P|$ = 2500 lbs.
Ω = 750 rad/sec

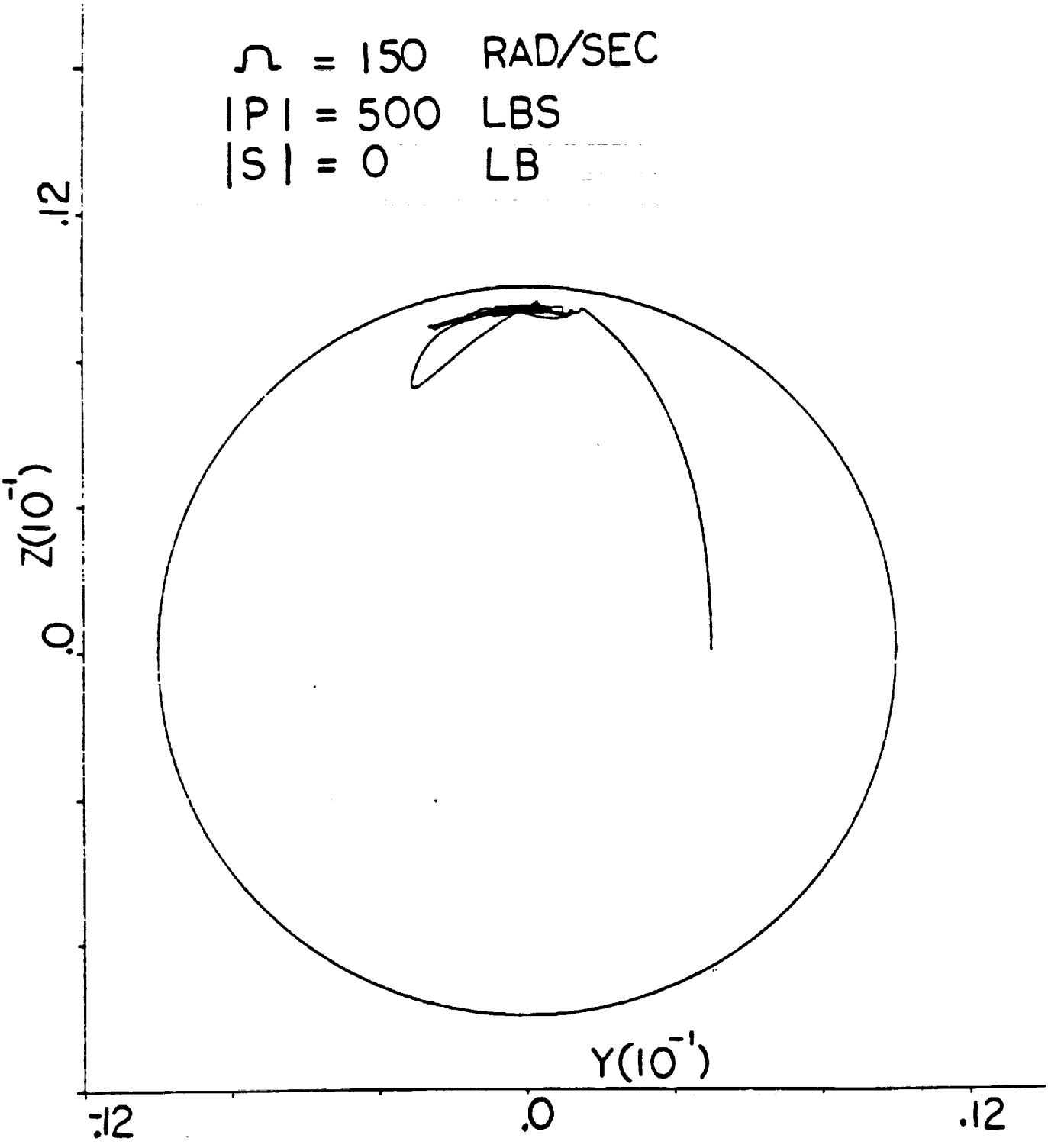

Fig. 25. Rotor Orbit;
$|P|$ = 2500 Lbs.
Ω = 750 rad/sec

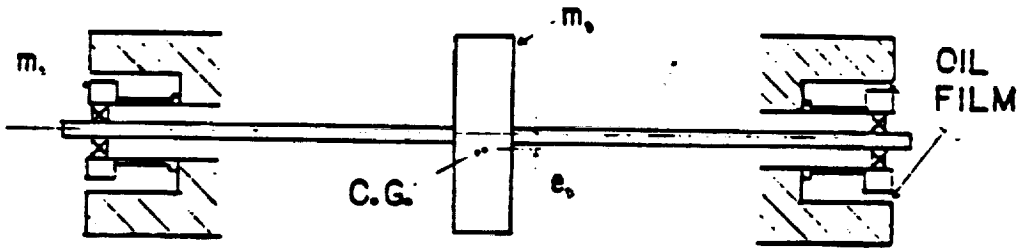

Figure 26. Symmetric, Lumped Mass Rotor with Damped, Flexible Supports

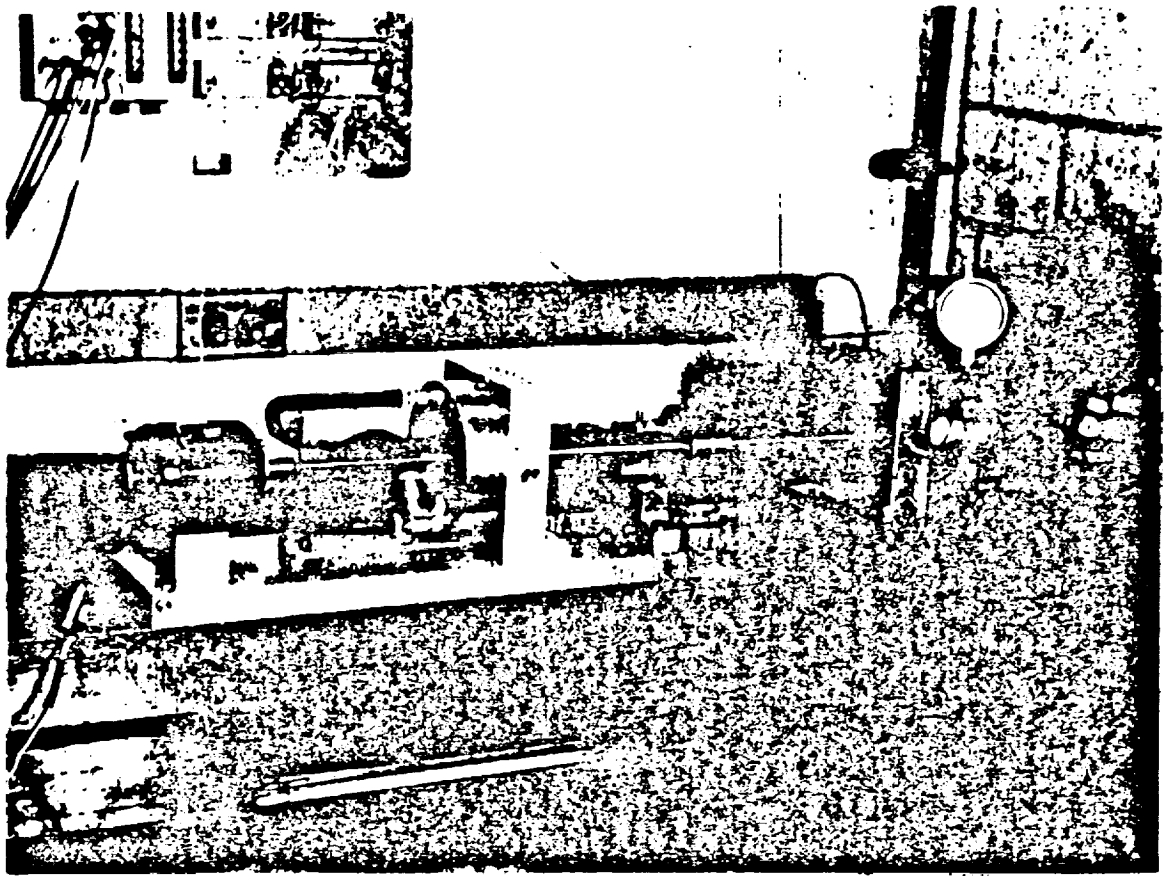

Figure 27. Experimental Test Facility Rotor

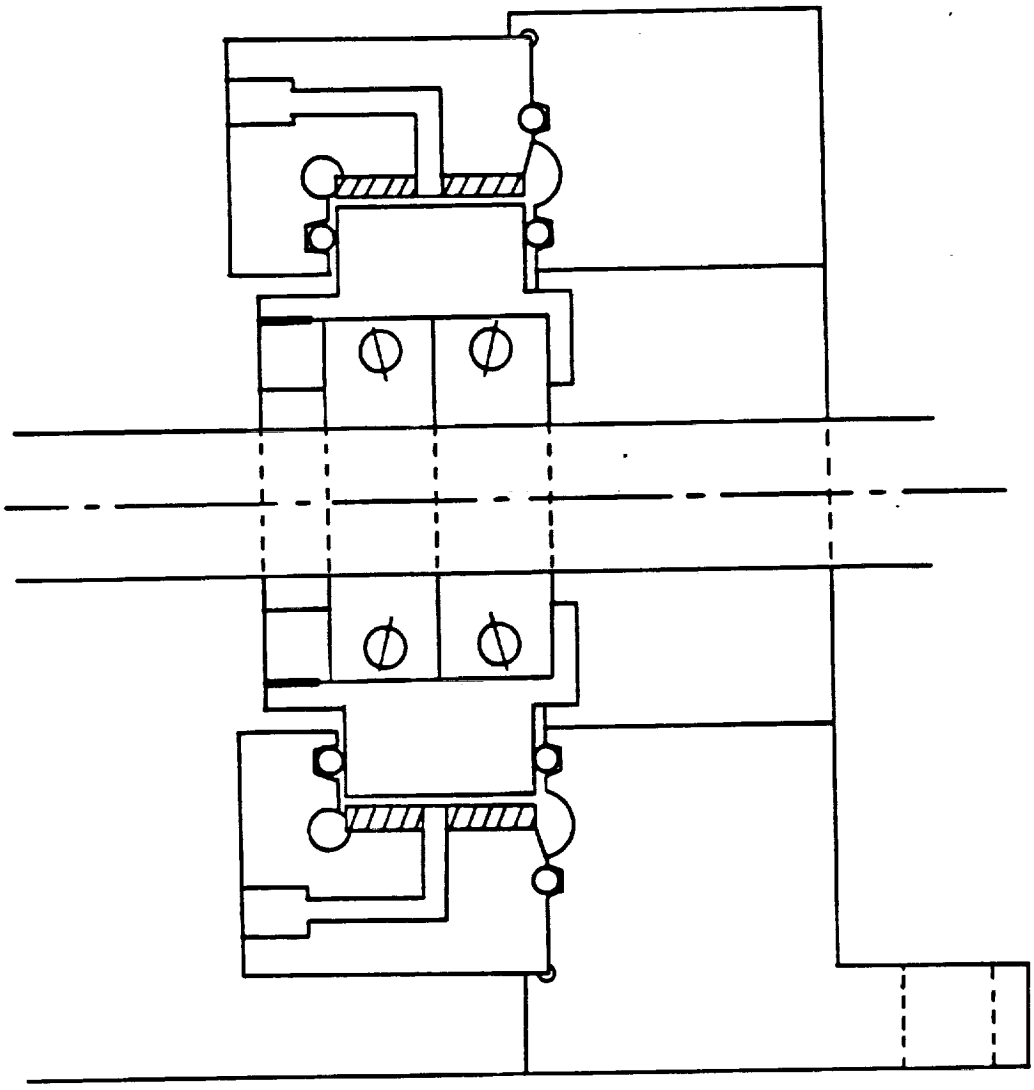

Figure 28. Schematic Side View of Experimental Damper Bearing Configuration

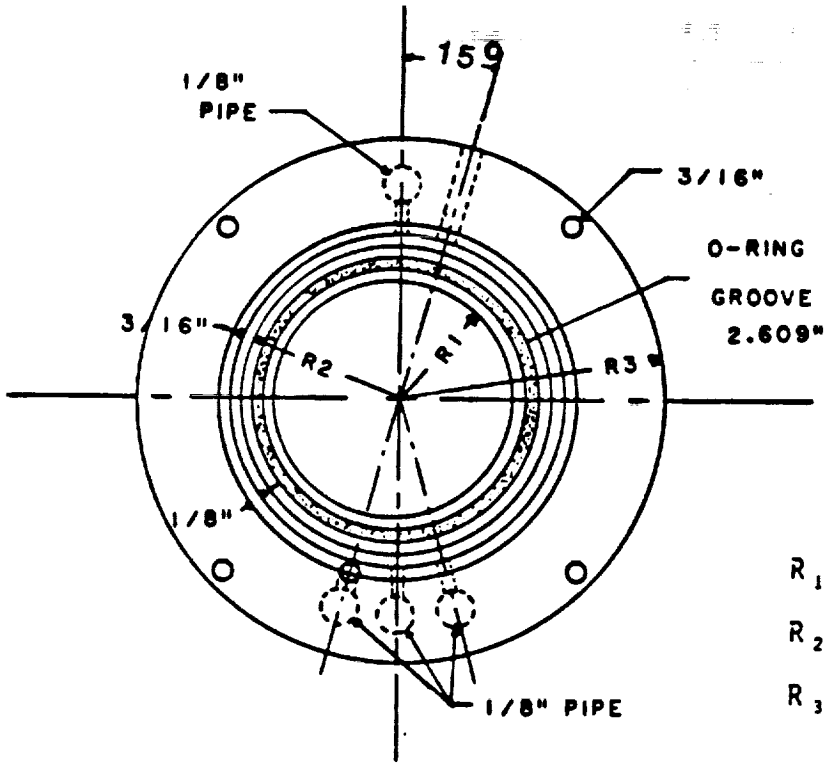

R_1 = 1-5/32"

R_2 = 1-19/32"

R_3 = 2-5/8"

1/2 Scale

Aluminum

2 Reqd.

Fig. 29. Damper Bearing

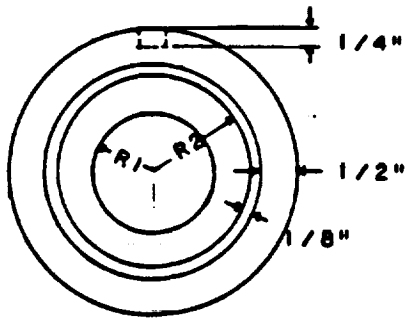

R_1 = .650"

R_2 = .9262"

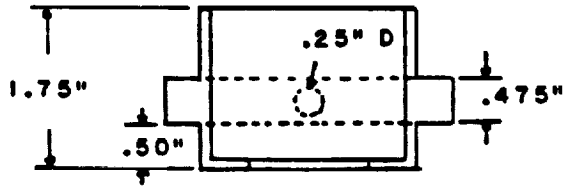

1/2 Scale

Aluminum

2 Reqd.

Fig. 30. Damper Journal/Bearing Holder

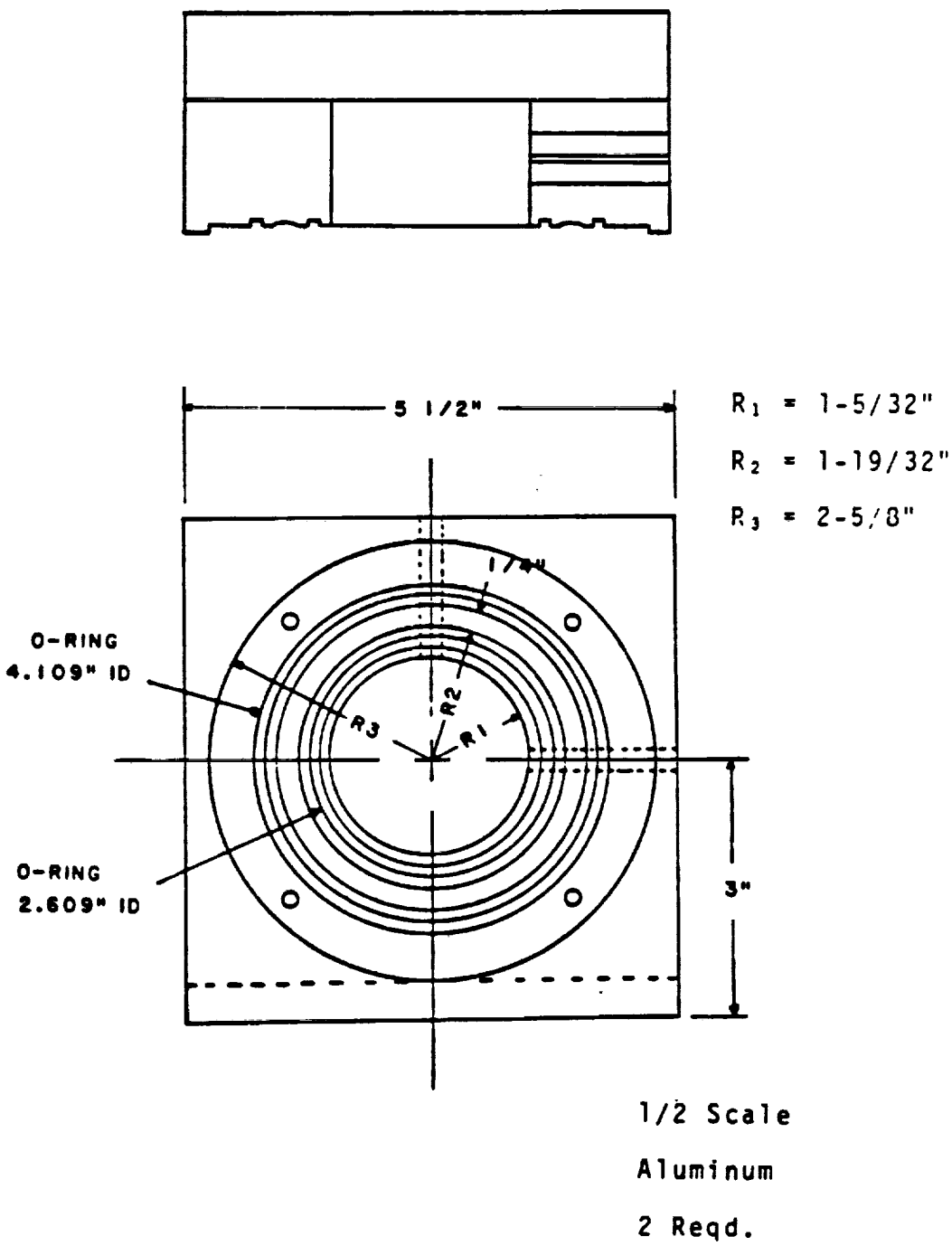

Figure 31. Bearing Housing

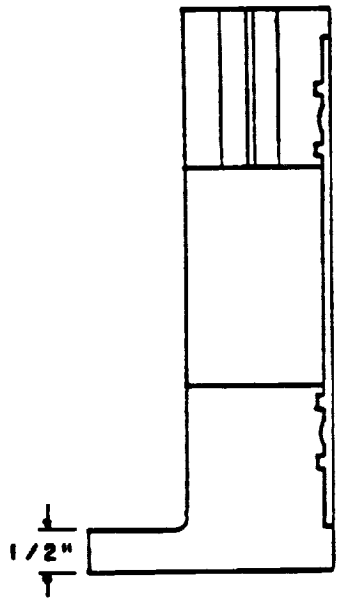

R_1 = 1-5/32"

R_2 = 1-19/32"

R_2 = 2-5/8"

1/2 Scale

Aluminum

2 Reqd.

Figure 32. Bearing Housing Side View

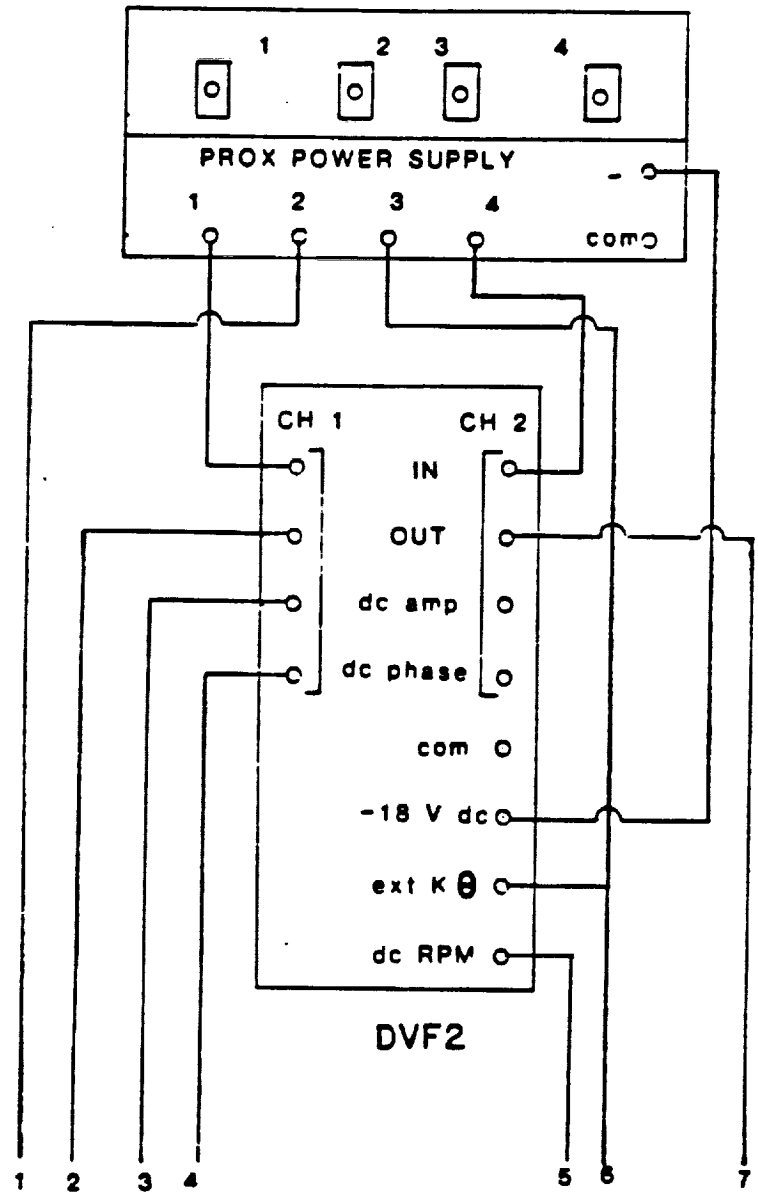

Figure 33. Wiring Schematic

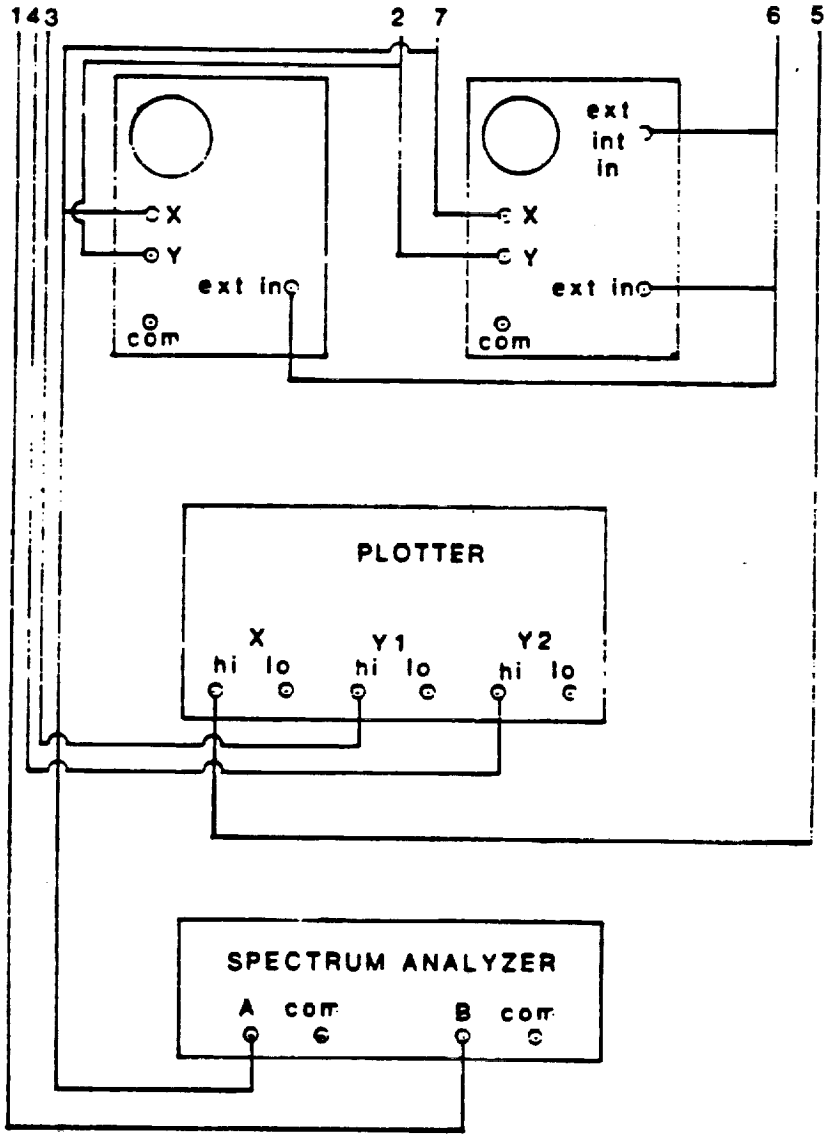

Figure 33. Wiring Schematic (Continued)

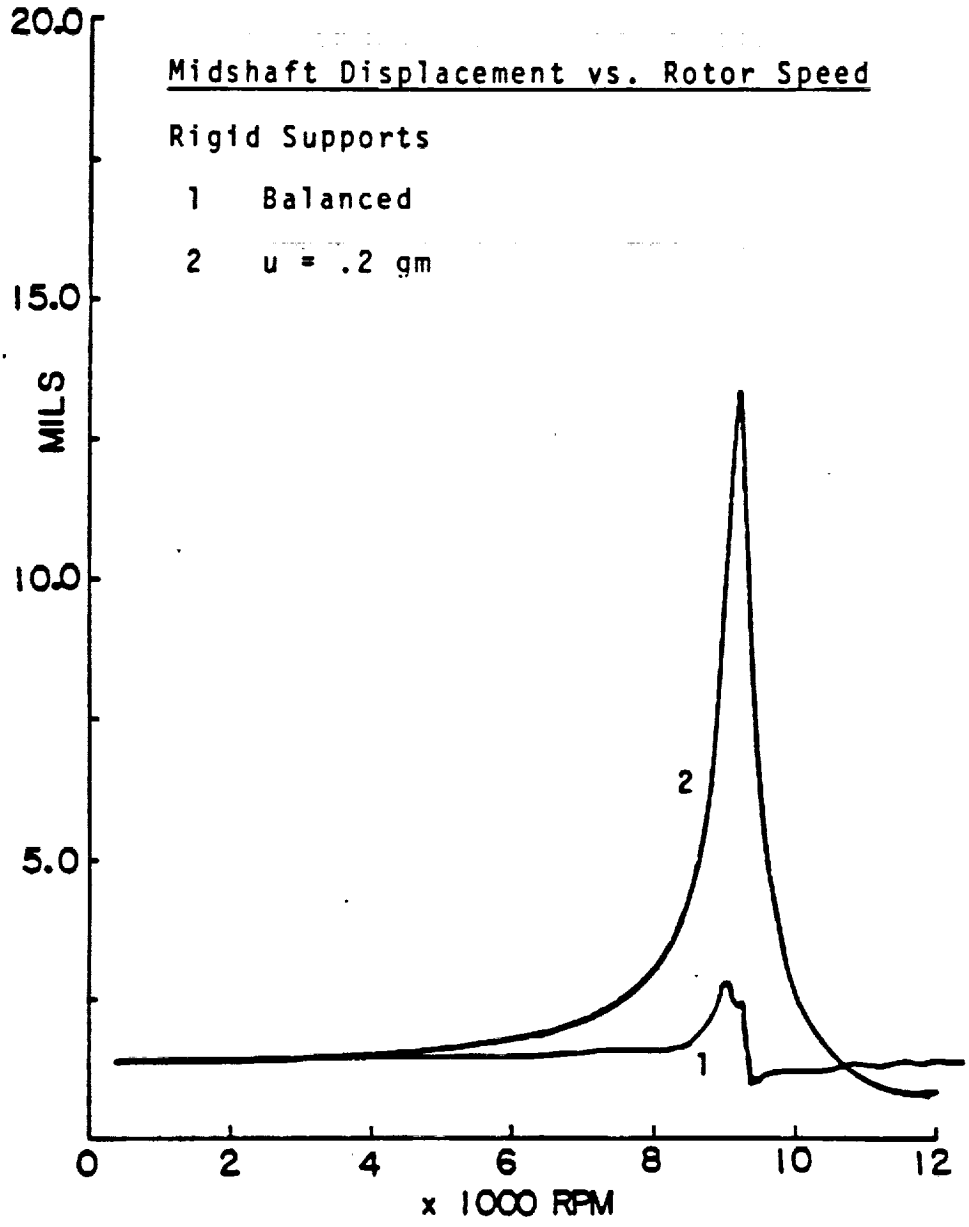
Midshaft Displacement vs. Rotor Speed
Rigid Supports
1 Balanced
2 u = .2 gm
20.0
15.0
10.0
5.0
MILS
0
2
4
6
8
10
12
x 1000 RPM
1
2

Figure 34

Midshaft Phase vs. Rotor Speed

Rigid Supports

u = .2 gm

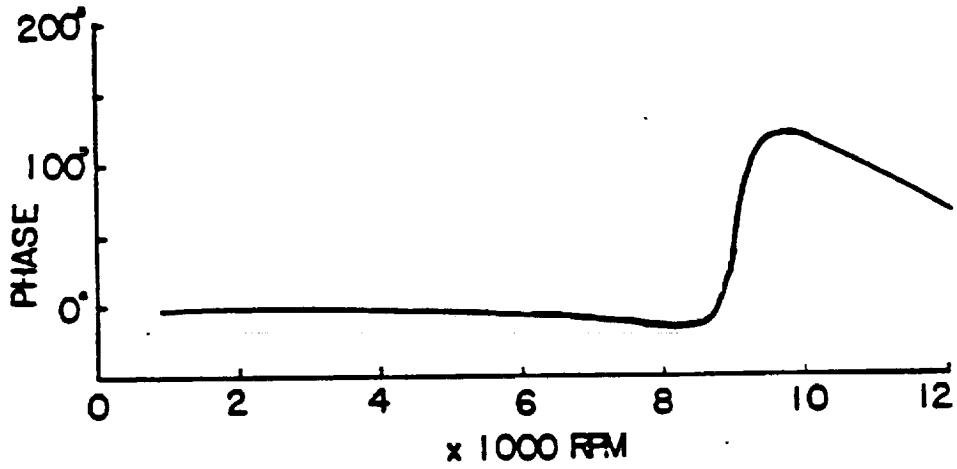

Figure 35

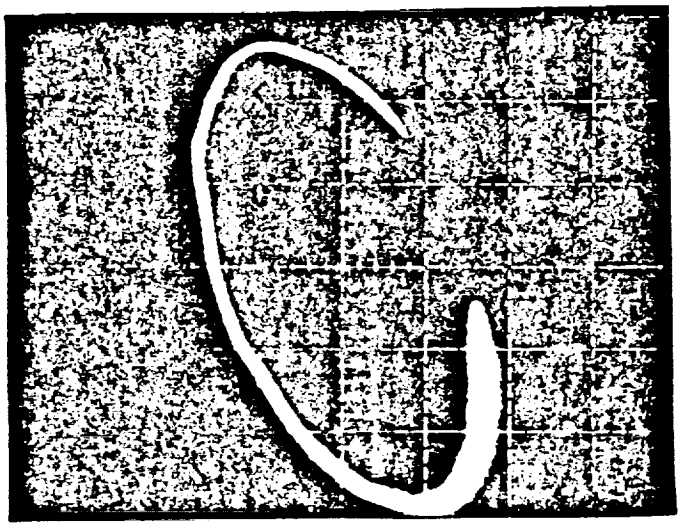

a. Damber Orbit, Groove Inlet, c = .01", 80°F, 9000 RPM, 10 psi, 3.0 gm unbalance, 1 MIL/DIV.

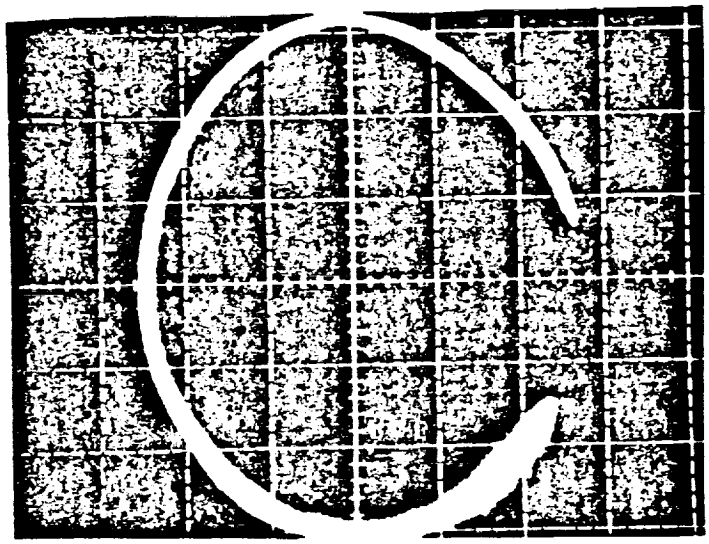

b. Shaft Orbit, same as above except 2 psi, 2.5 MIL/DIV.

Figure 36. Photographs of Oscilliscope Tracings of Damper and Shaft Orbits

Damper Orbits Relative to Clearance Circle

Groove Feed, 80°F, P_{in} = 2 psi, 9000 RPM

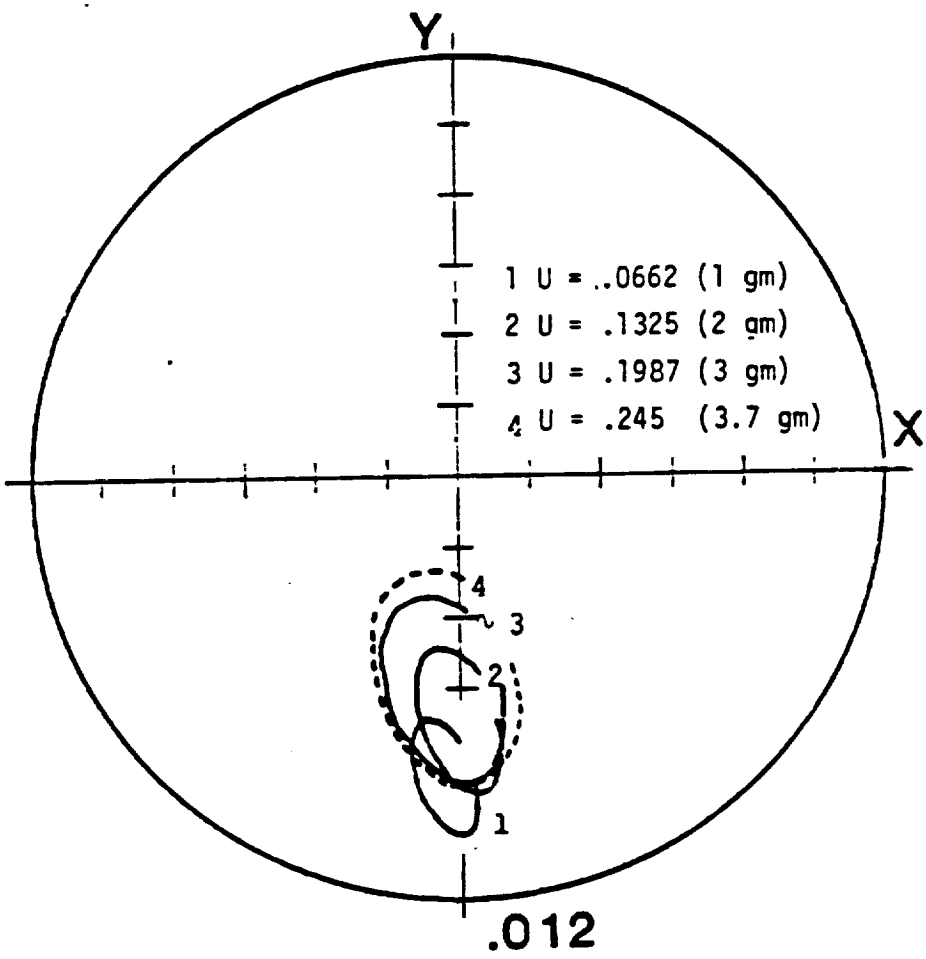

Figure 37

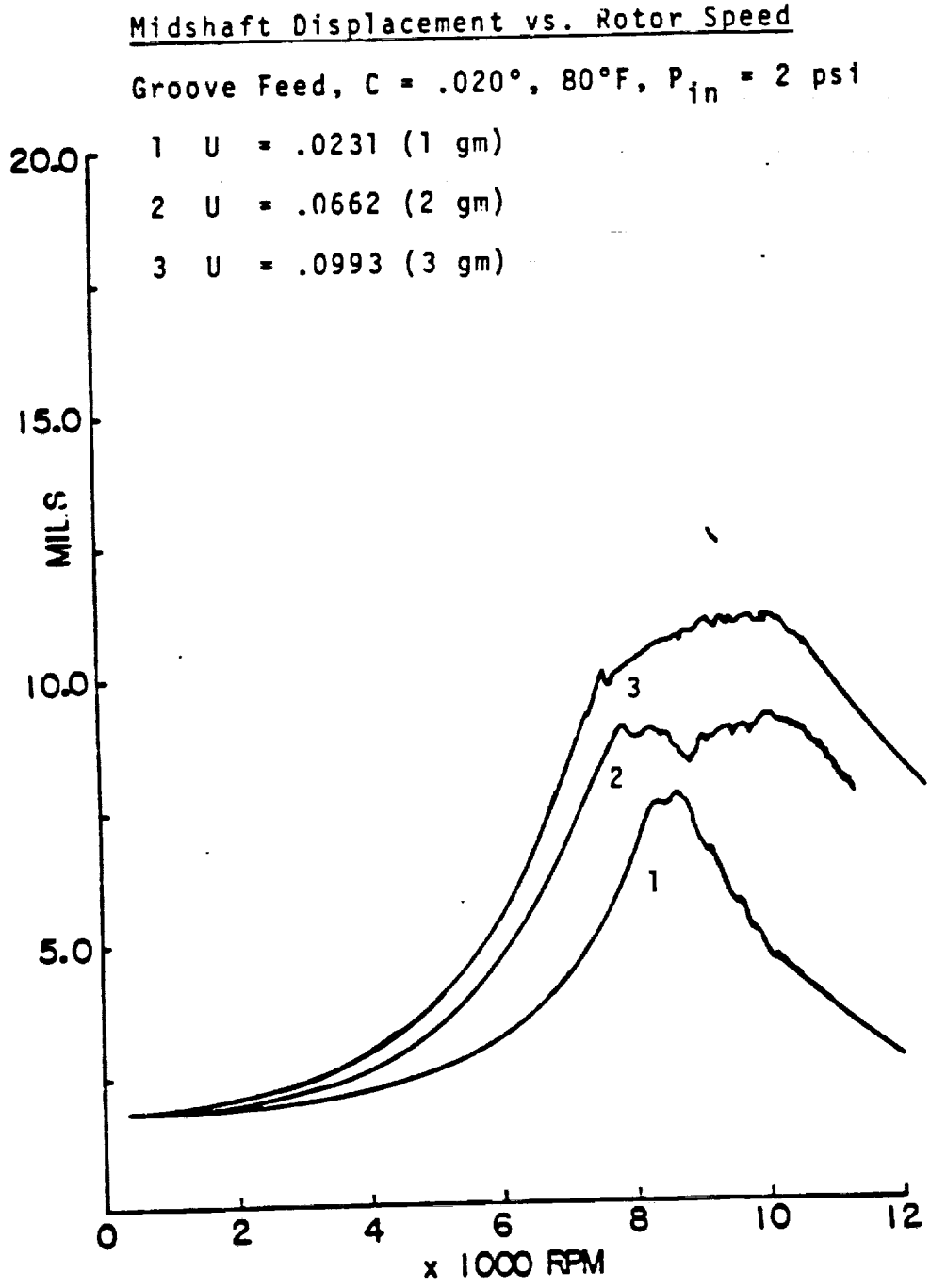
Midshaft Displacement vs. Rotor Speed
Groove Feed, C = .020°, 80°F, P_{in} = 2 psi
1 U = .0231 (1 gm)
2 U = .0662 (2 gm)
3 U = .0993 (3 gm)
20.0
15.0
10.0
5.0
MILS
3
2
1
0
2
4
6
8
10
12
x 1000 RPM

Figure 38

Midshaft Phase vs. Rotor Speed

Groove Feed, 80°F, C = .010", P_{in} = 2 psi

1 U = .0662 (1 gm)

2 U = .1987 (3 gm)

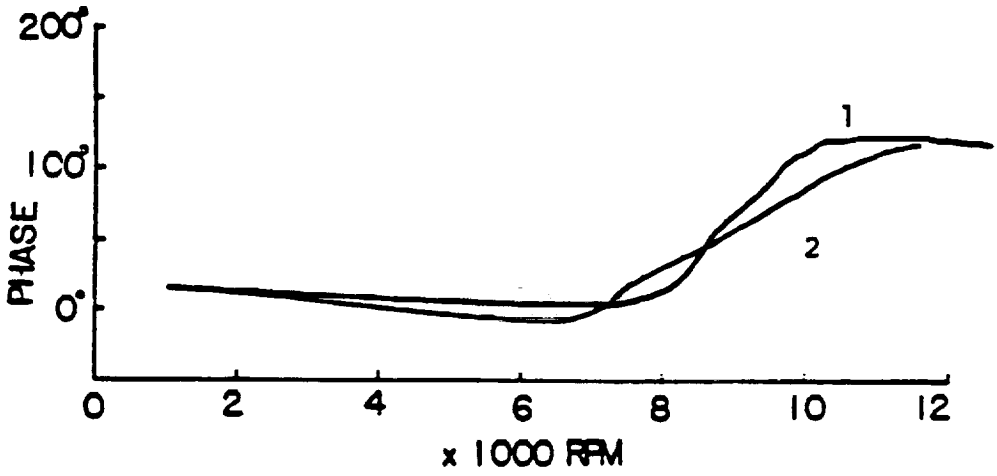

Figure 39

Midshaft Displacement vs. Rotor Speed

Groove Feed, C = .010", 80°F, P_{in} = 2 psi

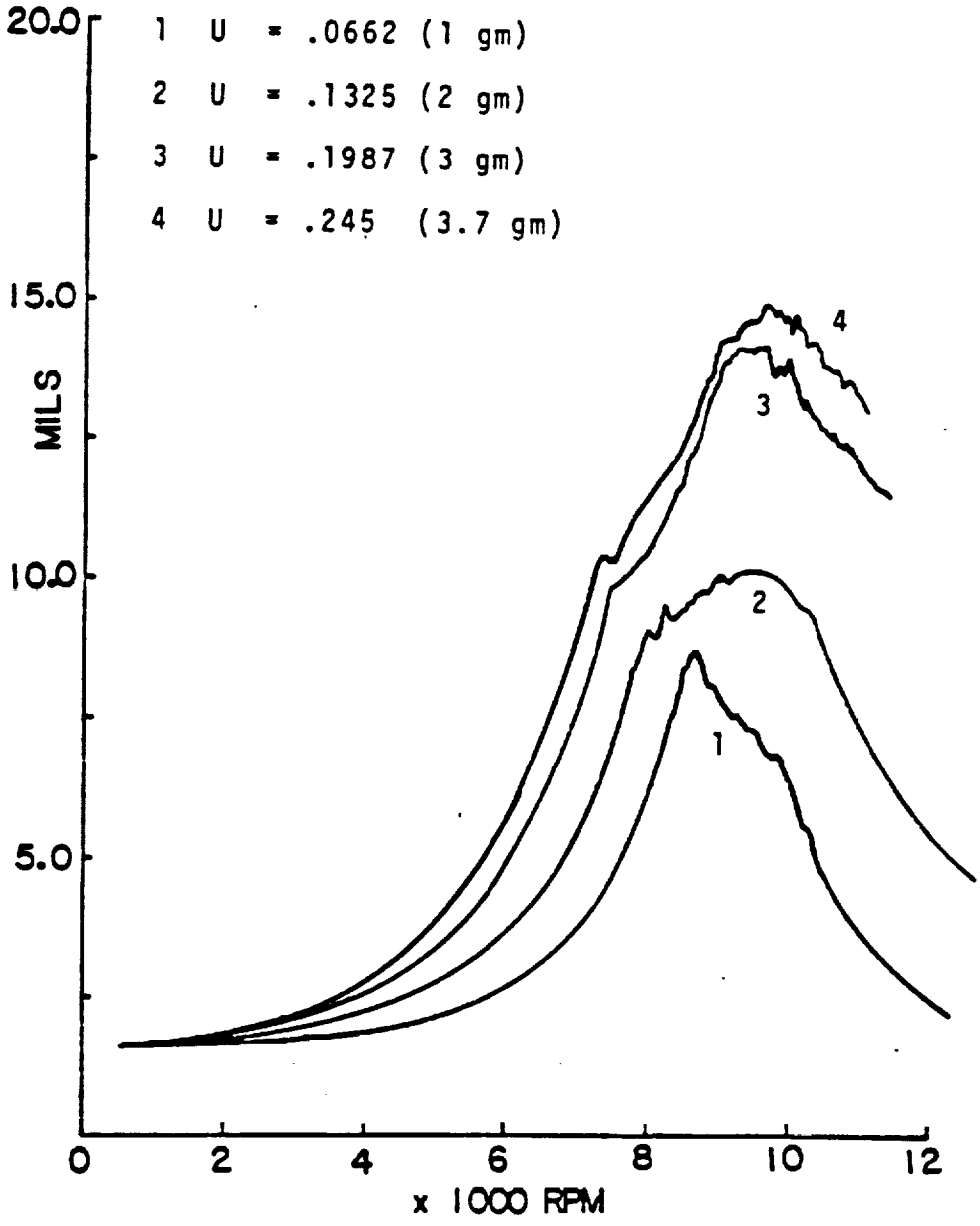

Figure 40

Midshaft Phase vs Rotor Speed

Groove Feed, 80°F, C = .006", P_{in} = 2 psi

1 u = 1 gm

2 u = 2 gm

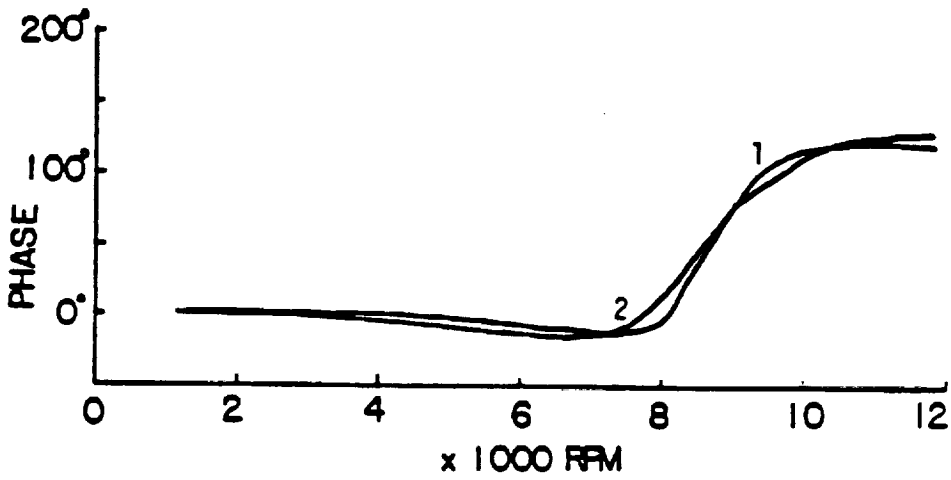

Figure 41

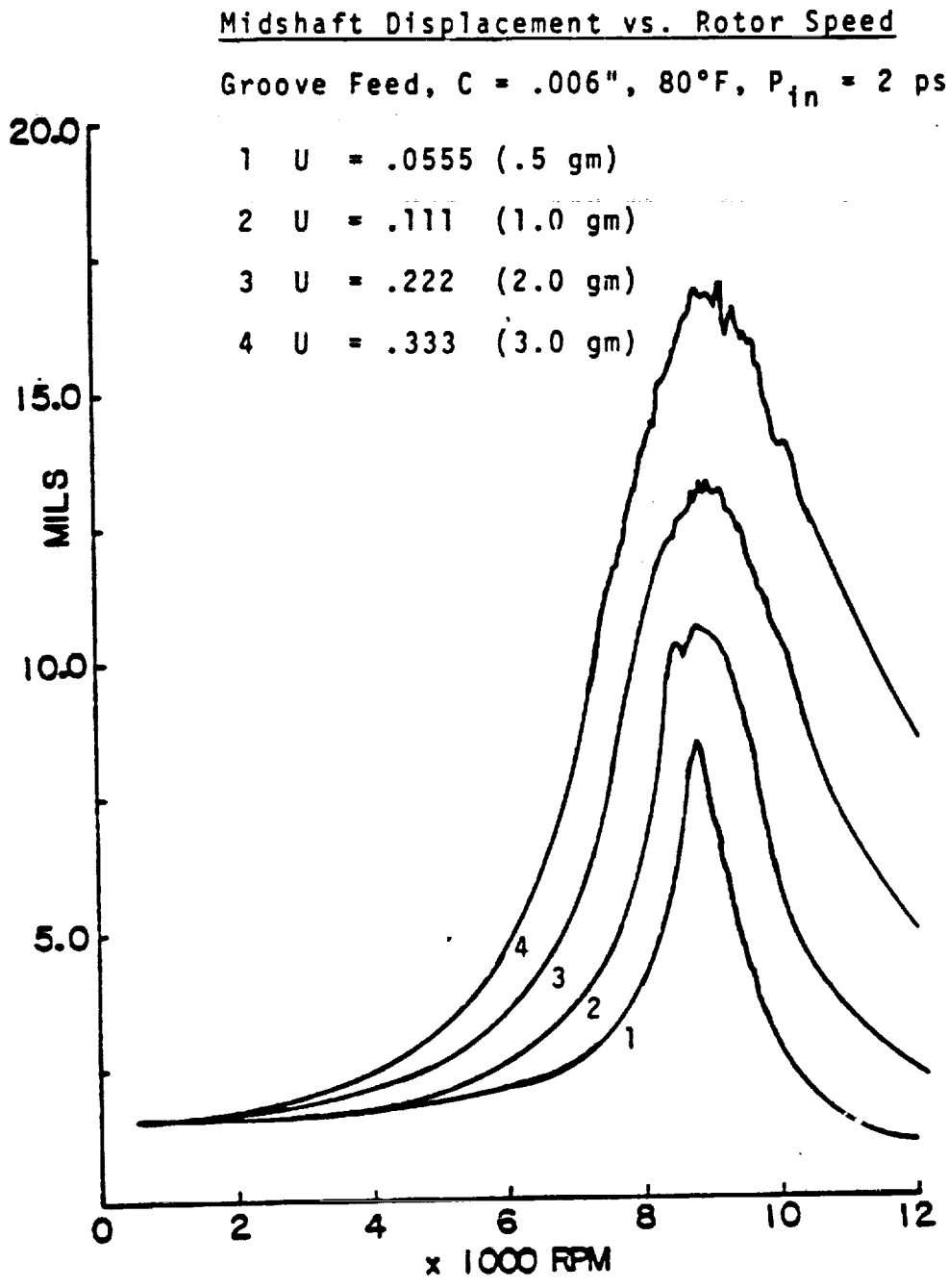
Midshaft Displacement vs. Rotor Speed
Groove Feed, C = .006", 80°F, P_{in} = 2 psi
1 U = .0555 (.5 gm)
2 U = .111 (1.0 gm)
3 U = .222 (2.0 gm)
4 U = .333 (3.0 gm)
20.0
15.0
10.0
5.0
MILS
0
2
4
6
8
10
12
x 1000 RPM
1
2
3
4

Figure 42

Damper Orbits Relative to Clearance Circle

Groove Feed, Low P_{in}, u = 3.2 gm, 10,000 RPM

1 $\mu = 10^{-6}$ Reyns. (160°F)

2 $\mu = 5x10^{-6}$ Reyns. (100°F)

3 $\mu = 10x10^{-6}$ Reyns. (80°F)

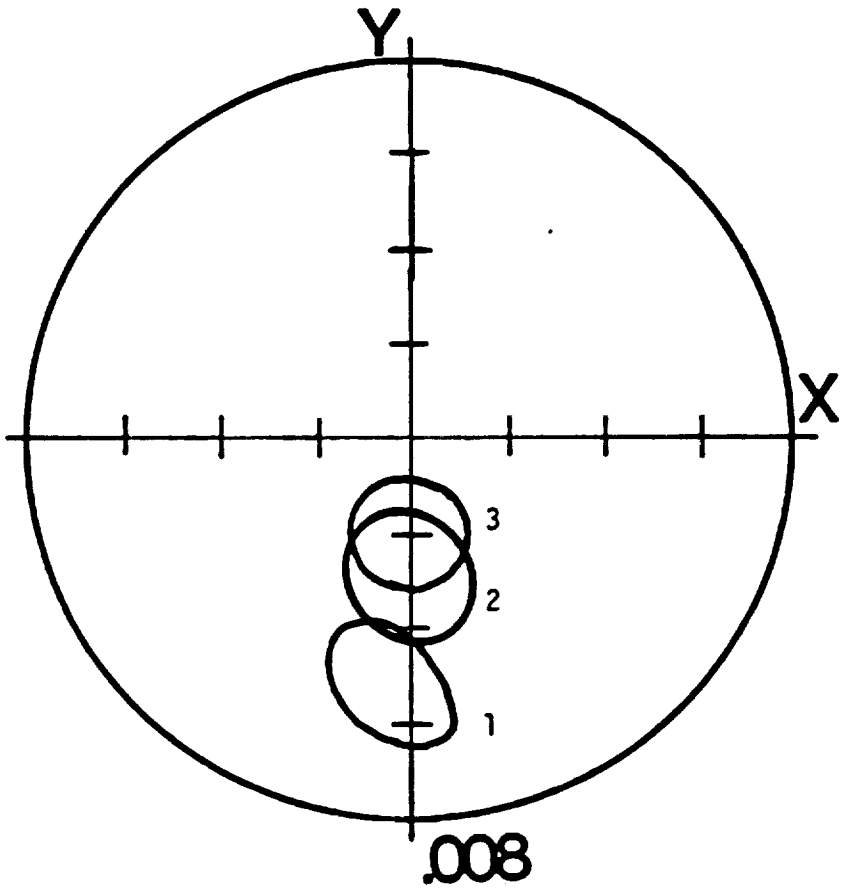

Figure 43

Damper Orbits Relative to Clearance Circle

Groove Feed, Low P_{in}, u = 3.2 gm, 10,000 RPM

1 10^{-6} Reyns. (160°F)

2 $5x10^{-6}$ Reyns. (100°F)

3 $10x10^{-6}$ Reyns. (80°F)

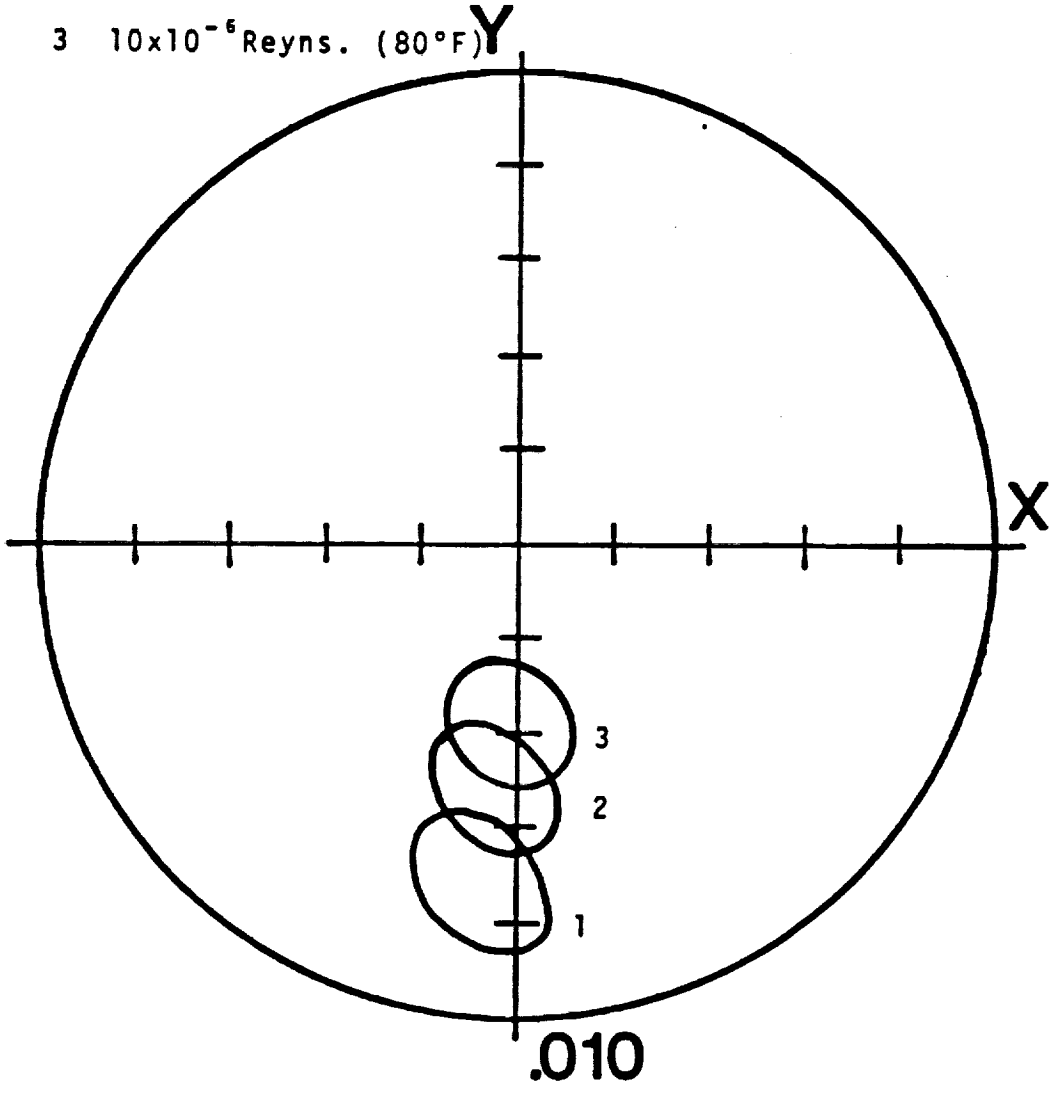

Figure 44

Damper Orbit Relative to Clearance Circle

Groove Feed, Low P_{in}, u = 3.2 gm, 10,000 RPM

1 10^{-6} Reyns. (160°F)

2 10×10^{-6} Reyns. (80°F)

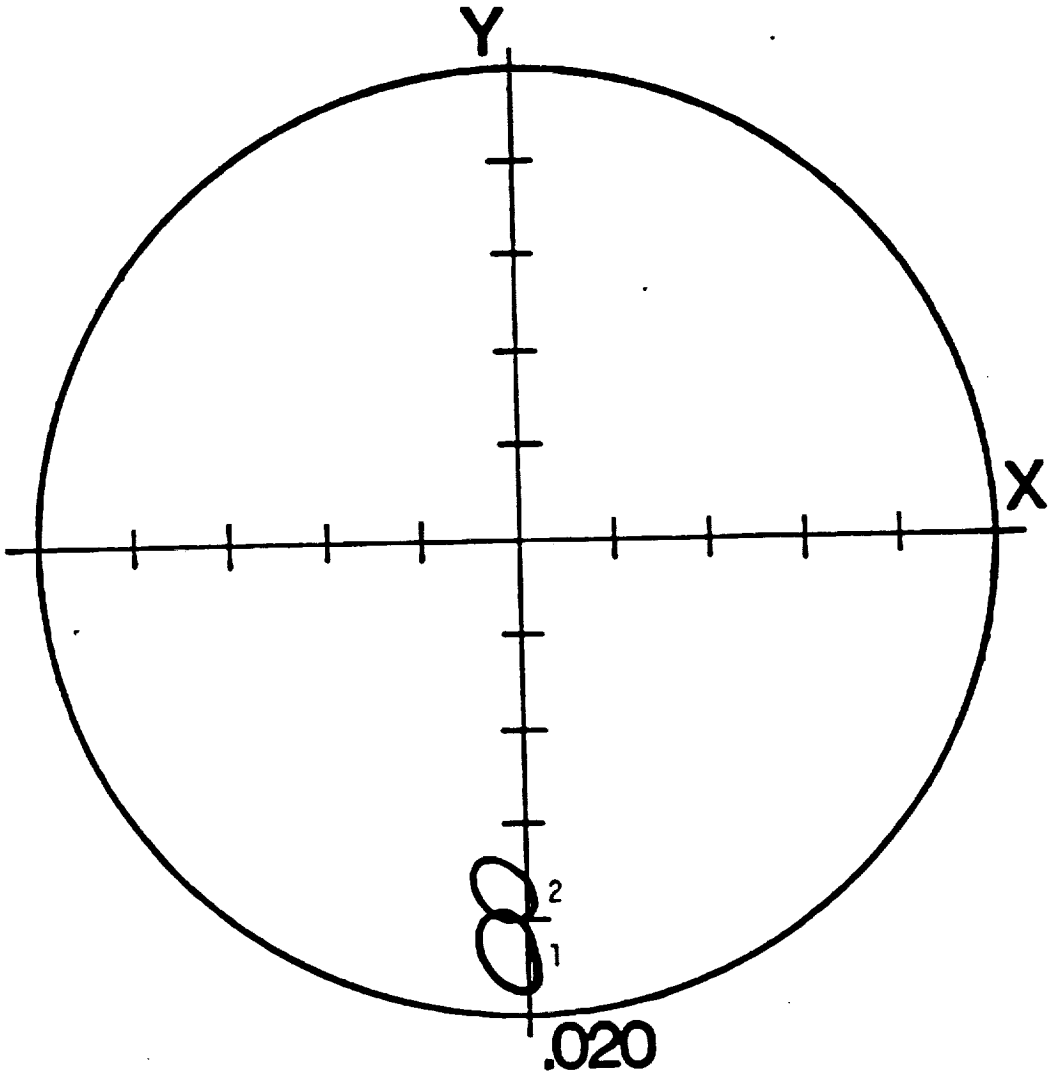

Figure 45

REPORT DOCUMENTATION PAGE

Form Approved
OMB No. 0704-0188

1. AGENCY USE ONLY (*Leave blank*)	2. REPORT DATE	3. REPORT TYPE AND DATES COVERED
	October 1991	Final Contractor Report

4. TITLE AND SUBTITLE
Engine Dynamic Analysis With General Nonlinear Finite Element Codes

5. FUNDING NUMBERS
WU-505-63-5B
G-NSG3-283

6. AUTHOR(S)
M.L. Adams, J. Padovan and D.G. Fertis

7. PERFORMING ORGANIZATION NAME(S) AND ADDRESS(ES)
University of Akron
Mechanical and Civil Engineering Departments
Akron, Ohio 44325

8. PERFORMING ORGANIZATION REPORT NUMBER
None

9. SPONSORING/MONITORING AGENCY NAMES(S) AND ADDRESS(ES)
National Aeronautics and Space Administration
Lewis Research Center
Cleveland, Ohio 44135-3191

10. SPONSORING/MONITORING AGENCY REPORT NUMBER
NASA CR-187222

11. SUPPLEMENTARY NOTES
Project Manager, C.C. Chamis, Structures Division, NASA Lewis Research Center, (216) 433-3252.

12a. DISTRIBUTION/AVAILABILITY STATEMENT
Unclassified - Unlimited
Subject Category 39

12b. DISTRIBUTION CODE

13. ABSTRACT (*Maximum 200 words*)

A general engine dynamic analysis as a standard design-study computational tool is described for the prediction and understanding of complex engine dynamic behavior. Improved definition of engine dynamic response provides valuable information and insights leading to reduced maintenance and overhaul costs on existing engine configurations. Application of advanced engine dynamic simulation methods provide a considerable cost reduction in the development of new engine designs by eliminating some of the trial-and-error process done with engine hardware development.

14. SUBJECT TERMS
Finite element; Computer code; Engine dynamics; Comparisons; Multi-bearings; Flexible

15. NUMBER OF PAGES
92

16. PRICE CODE
A05

17. SECURITY CLASSIFICATION OF REPORT	18. SECURITY CLASSIFICATION OF THIS PAGE	19. SECURITY CLASSIFICATION OF ABSTRACT	20. LIMITATION OF ABSTRACT
Unclassified	Unclassified	Unclassified	